

Linkages between East China Sea Deep-sea Oxygenation and Variability in the East Asian Summer Monsoon and Kuroshio Current over the last 400,000 years

Nishant Vats^{1*}, Raj K. Singh^{1*}, Manisha Das¹, Ann Holbourn², Anil K. Gupta³, Stephen J. Gallagher⁴ and D. K. Pandey⁵

¹School of Earth, Ocean and Climate Sciences, Indian Institute of Technology Bhubaneswar, Argul, Jatni – 752050, India.

²Institute of Geosciences, Christian-Albrechts-University of Kiel, Ludewig-Meyn-Str. 14, D-24118 Kiel, Germany.

³Department of Geology and Geophysics, Indian Institute of Technology Kharagpur, Kharagpur – 721302, India

⁴School of Earth Sciences, University of Melbourne, Melbourne, Australia.

⁵ESSO-National Centre for Polar and Ocean Research, Goa - 403804, India.

*Corresponding author: Nishant Vats (nv11@iitbbs.ac.in)

Raj K. Singh (rk Singh@iitbbs.ac.in)

Key Points:

- Four distinct phases of bottom water oxygenation identified during the last 400 kyr in the East China Sea.
- East Asian Summer Monsoon and Kuroshio Current influence East China Sea productivity, organic export flux and bottom water oxygenation.
- Precessional variability modulates bottom water oxygenation in ECS.

Abstract

The East China Sea (ECS) seasonally receives a high organic input due to the terrestrial organic matter influx, which is controlled by the East Asian Summer Monsoon (EASM), and the increased productivity driven by upwelling of the subsurface Kuroshio Current (KC). Changes in benthic foraminiferal assemblage composition in combination with paleoceanographic proxy data (CaCO_3 (%), TOC (%), $\delta^{13}\text{C}_{\text{pf}}$, and $\delta^{18}\text{O}_{\text{bf}}$) are used to reconstruct bottom water oxygenation and organic export flux variability over the last 400 kyr in the ECS. Multivariate analyses of benthic foraminiferal census data identified six biofacies characteristic of varying environmental conditions. These results suggest that enhanced EASM precipitation and KC upwelling directly influenced organic export flux and bottom water oxygen content in the ECS. The ECS bottom water was suboxic during Marine Isotope Stage (MIS) 11 to 8; suboxic to dysoxic between MIS 7 and 6, strongly dysoxic between mid-MIS 5 and 4, and exhibited high variability between MIS 3 and 1. Spectral analysis of relative abundances of representative genera *Quinqueloculina* (oxic), *Bulimina* (suboxic), and *Globobulimina* (dysoxic) reveals a robust 23 kyr signal, which we attribute to precessionally-paced changes in surface productivity and bottom water oxygenation related to EASM and KC variability over the past 400 kyr.

Keywords: IODP Site U1429, Bottom water oxygenation, Precessional variability, East China Sea, Benthic foraminifera

1 Introduction

Deep-sea oxygenation of the East China Sea (ECS) is influenced by deep water circulation (Kao et al., 2005; Lim et al., 2017) and subsurface intrusion of the Kuroshio Current (KC) (P. Zhou et al., 2018a, b). Kuroshio intensification enhances deep water circulation and adds oxygen to the sediment-water interface (Kao et al., 2005; Lim et al., 2017), whereas upwelling of nutrient-rich subsurface Kuroshio water in the ECS drives higher productivity along the Zhejiang coast in the ECS (Chen & Wang, 1999; Zhang et al., 2007), promoting the decline in dissolved oxygen (P. Zhou et al., 2018b). Thus, deep-water circulation, primary productivity and the upwelling of the subsurface KC are the primary processes that contribute to dissolved oxygen in the ECS (Gallagher et al., 2009, 2015). Productivity in the upper water column of the ECS is also linked to nutrient arrival associated with the East Asian Summer Monsoon (EASM) (J. Hu & Wang, 2016; Watanabe et al., 2007). The influx of terrestrial organic matter in the ECS is regulated by active river

discharge and run-off associated with seasonal EASM precipitation variability (Lee et al., 2001; Matsuzaki et al., 2016). This further affects primary productivity and may contribute to the higher rate of organic matter sinking to the sea floor. Today, hypoxia occurs in the Changjiang Estuary of the ECS during the summer season (Fig. 1; D. Li et al., 2002; B. Wang, 2009; B. Wang et al., 2012), which coincides with seasonal EASM riverine influx and KC influx in the ECS. The water column stratification and dissolved oxygen consumption by organic matter promote hypoxia formation in the ECS (D. Li et al., 2002; Wei et al., 2007; Zhu et al., 2011). The oxygen utilization profile of the Okinawa Trough (OT) in the ECS also suggests a higher rate (~ 5.3 ml/l) of dissolved oxygen consumption at the sediment water-interface (Fig. S1(a)). It is likely that the influence of EASM driven productivity and KC upwelling also varied on glacial-interglacial and shorter time scales. The long-term evolution of bottom water oxygenation has been reconstructed for the South China Sea (N. Wang et al. 2018) and Japan Sea (Manisha Das et al. 2021), using benthic foraminiferal proxies. In the ECS, Matsuzaki et al. (2019) used the deep-dwelling planktic radiolarian species *Cycladophora davisiana* to reconstruct sub-surface oxygenation. However, as a planktic species, this taxon cannot be used to estimate oxygenation at the sediment-water interface nor to monitor the variability in suboxic to dysoxic conditions during climate transition phases. Furthermore, the relative abundance of *C. davisiana* is generally low ($\sim 5\%$) between MIS 11 and MIS 6 and rare in strata younger than MIS 6 (Matsuzaki et al., 2019). Other deep-sea oxygenation reconstructions in the ECS and OT are only available back to the Last Glacial Maximum (LGM) (Kao et al., 2005; Lim et al., 2017). Hence, the factors influencing deep-sea oxygenation in the ECS and OT on longer time scales are yet to be fully understood. Thus, it is crucial to reconstruct long-term bottom water oxygenation for ECS over several glacial-interglacial cycles to better understand sub-orbital and orbital variability.

Various proxies have been used to assess variability in deep-water oxygenation including the benthic foraminiferal oxygen index (BFOI) (Kaiho, 1994, 1999; Kaminski, 2012; N. Wang et al., 2018), Mo/Al (N. Wang et al., 2018), I/Ca (Taylor et al., 2017), the number of pores in epifaunal benthic foraminifera (Rathburn et al., 2018), the grey color reflectance index (L^*) (Huang et al., 2019; Irino et al., 2018; Kido et al., 2007; Tada et al., 1999; Watanabe et al., 2007). Benthic foraminifera inhabit the seafloor near sediment-water interface and are useful proxies to assess bottom water oxygenation (e.g., Burkett et al., 2016; Moumita Das et al., 2017; Lutze & Thiel, 1989; Rathburn et al., 2018). Surface productivity and the associated organic matter flux to

the seafloor as well as the dissolved oxygen content in bottom water are major factors controlling the distribution of particular species of benthic foraminifera (e.g., Moumita Das et al., 2017; Fontanier et al., 2002; Jorissen et al., 2007; Sen Gupta & Machain-Castillo, 1993; Y. Zhou et al., 2016). The abundance, diversity and habitat (epifaunal, shallow infaunal and deep infaunal) of benthic foraminifera as well as the size and chemical composition of tests vary with bottom water conditions (Barik et al., 2019; Rathburn et al., 2018). Jorissen et al. (2007) suggested that foraminiferal diversity and density, in particular, are strongly influenced by the availability of food and the oxygenation of bottom and sediment pore water. Therefore, benthic foraminifera provide ideal proxies to retrace the evolution of bottom-water oxygenation and the organic export flux to the sea floor through time.

This study uses benthic foraminiferal assemblages from Integrated Ocean Drilling Program (IODP) Site U1429 to reconstruct shifts in bottom water oxygenation and variability in organic export flux in the ECS over the last 400 kyr. Multivariate analysis and environmental preferences of benthic foraminifera are used in addition to total organic carbon (TOC wt. %) and CaCO_3 (%) data (Black et al., 2018), the radiolarian species *Cycladophora davisiana* abundance (%) (Matsuzaki et al., 2019), planktic foraminiferal $\delta^{13}\text{C}$ values ($\delta^{13}\text{C}_{\text{pf}}$) and benthic foraminiferal $\delta^{18}\text{O}$ values ($\delta^{18}\text{O}_{\text{bf}}$) (Clemens et al., 2018) from the same site.

2 Site Location and Oceanographic Setting

IODP Site U1429 (31°37.04'N, 128°59.85'E) (Fig. 1) in the ECS was cored down to 182 meters below sea floor (mbsf) at a water depth of 732 meters below sea level (mbsl; Tada et al., 2015). This site is located in the Danjo Basin on the western continental slope of the northern OT in the northeastern ECS (Fig. 1). The sediment succession at this site is mainly composed of calcareous nannofossil ooze and calcareous nannofossil-rich clay (Tada et al., 2015; D. Zhao et al., 2019). The KC and the Taiwan warm Current (TC) strongly influence the surface and subsurface waters of the ECS (e.g., Matsuzaki et al., 2016), respectively. The KC intrusion into the ECS is seasonally controlled by volume transport fluctuations (Z. Liu et al., 2021; P. Zhou et al., 2018b) in the transport of warm, highly saline waters from low to middle latitudes (D. Hu et al., 2015; D. Zhao et al., 2017; Zheng et al., 2016). The KC brings oxygen-rich, warm, saline and oligotrophic water to the ECS from the north equatorial Pacific region (Gallagher et al., 2015; Lee et al., 2001; Matsuzaki et al., 2019, 2016; Vats et al., 2020), while subsurface KC-driven upwelling

(Chen et al., 1995; K. K. Liu et al., 1992; Vats et al., 2020; Wu et al., 2008; P. Zhou et al., 2018a) brings nutrients and influences primary productivity. The nutrient rich TC flows in to the ECS (Matsuzaki et al., 2019) from the Taiwan strait and increases the productivity in the continental shelf areas of the ECS, however, its influence gets restricted to the western part of the ECS. It flows northward throughout the year, even during winter, with strong northerly winds (Ji-lan et al., 1994; Qi et al., 2017).

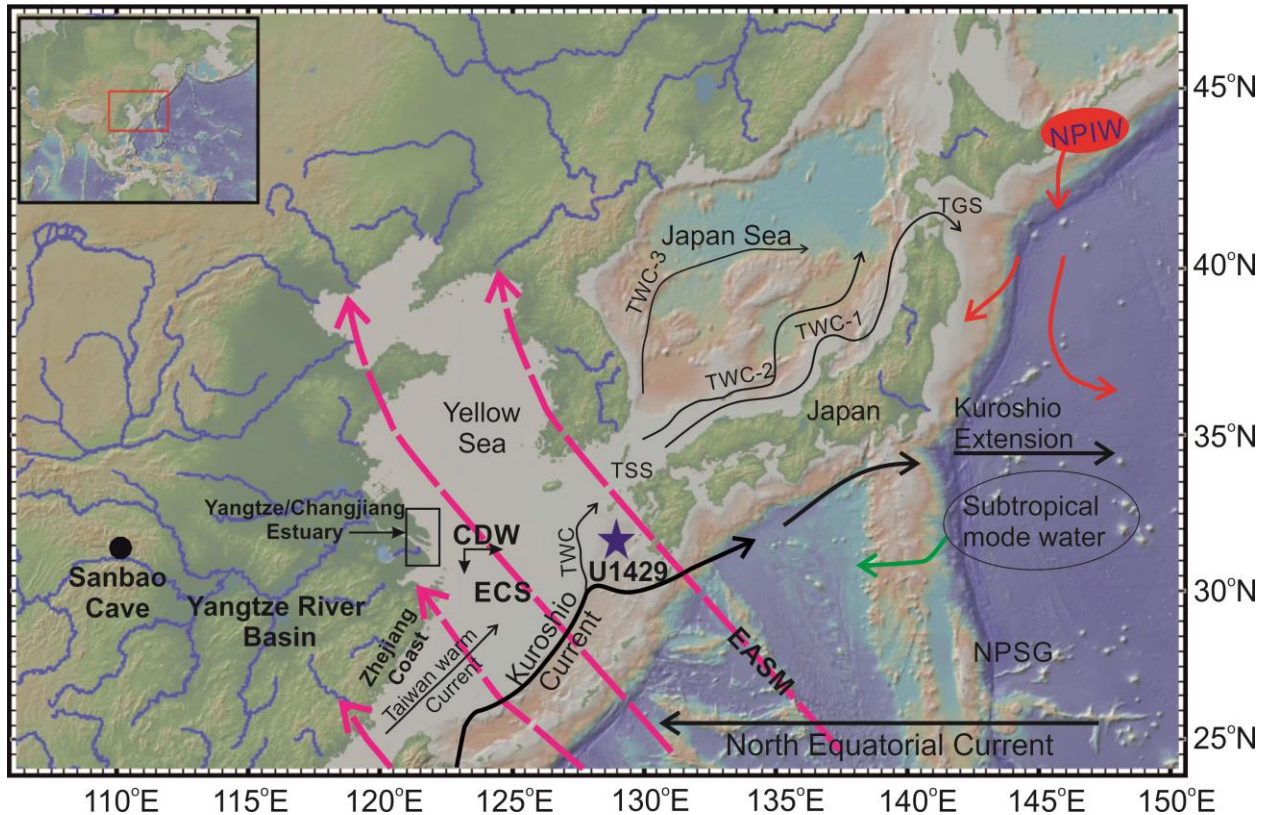


Figure 1. Location of IODP Site U1429 (31°37.04'N, 128°59.85'E, 732 mbsl) in the East China Sea (Blue star). Location of the Sanbao cave in China (Filled black circle). Black arrows indicate surface current directions. Magenta arrows indicate the East Asian Summer Monsoon (EASM) direction. CDW– Changjiang Diluted Water, NPIW– North Pacific Intermediate Water, TWC– Tsushima Warm Current, NPSG– North Pacific Subtropical Gyre, TSS– Tsushima Strait, TGS– Tsugaru Strait. Surface currents marked after D. Zhao et al. (2017) and EASM direction marked after N. Li et al. (2021). This map was made with GeoMapApp (<http://www.geomapapp.org>) using the GMRT data set (Ryan et al., 2009).

The other major component in the ECS is the Changjiang Diluted Water (CDW), which brings freshwater from northwestern China and lowers the salinity and temperature in the ECS (Ichikawa & Beardsley, 2002). The CDW is associated with EASM precipitation, and its influence is seasonal (Lee et al., 2001; Matsuzaki et al., 2016). The CDW discharge also brings nutrients affecting biological productivity and the accumulation of terrestrial organic matter in the ECS. The sinking of organic matter to the bottom of the ECS consumes the available bottom water dissolved oxygen. Hence, enhanced subsurface KC upwelling and stronger EASM strongly influence bottom water oxygenation in the ECS. The modern annual oxygen utilization and dissolved oxygen concentration at the sediment-water interface near to the studied site is ~5.3 ml/l and ~1.6 ml/l, respectively (Fig. S1(a-b); Garcia et al., 2013). The decadal average (1955-2017) bottom water temperature and salinity at sediment-water interface are ~4°C (Fig. S1(c); Locarnini et al., 2019) and ~34.35 (Fig. S1(d); Zweng et al., 2019), respectively.

3 Materials and Methods

A total of 225 sediment core samples (of 10 cc volume) were analyzed from IODP Site U1429, down to 182 mbsf. We used the high-resolution age model published by Clemens et al. (2018), which shows that the sediment succession extends back to ~400 ka. The upper part of the succession (back to 40 ka) was further constrained by 16 AMS ^{14}C dates (10 from Vats et al., 2020 and 6 from D. Zhao et al., 2017). The average temporal resolution per sample is ~2 kyr (Vats et al., 2020). The same age model was also used to plot TOC (%), CaCO_3 (%) (Black et al., 2018), $\delta^{13}\text{C}_{\text{pf}}$ and $\delta^{18}\text{O}_{\text{bf}}$ (Clemens et al., 2018) and the *Cycladophora davisiana* (%) abundance data (Matsuzaki et al., 2019). Out of 225 samples, 36 samples yielded fewer than 30 specimens of foraminifera per 10 cc sediment, and these samples were discarded from the statistical analysis, as they may lead to artefacts. Most of these discarded samples are from the tephra layers within the core (Sagawa et al., 2018; Tada et al., 2015).

The samples were processed and analyzed following the standard methods outlined by Manisha Das et al. (2018). Benthic foraminiferal census data were generated for each sample from the >125 μm size fraction, and species abundance (percentage) was calculated. Benthic foraminiferal classification follows Loeblich and Tappan (1988) at the genus level and Manisha Das et al. (2018, 2021), Gallagher et al. (2018), Holbourn et al. (2013), Scott et al. (2000), and

Zwaan et al. (1986) at the species level. Two hundred thirty-six species of benthic foraminifera belonging to 96 genera were identified.

Of the 236 species identified, only 32 species (Fig. 2) with an abundance of $\geq 5\%$ in 5 or more samples were selected for multivariate analysis. Exploratory factor analysis was performed on these species and to maximize the variance “fa” function and “pa” method (principal axes) of Psych package (Revelle, 2019; RStudio Team, 2020) were used. Based on scree-plot (X-Y) of eigenvalues, five factors were retained. Hierarchical cluster analysis was performed using Ward’s minimum linkage method for the same 32 species, which enabled to retain 6 clusters (Manisha Das et al., 2021; RStudio Team, 2020; R. K. Singh et al., 2021; Fig. S2). Incorporating consistent results from exploratory factor analysis and hierarchical cluster analysis, six biofacies of benthic foraminifera were identified in the ECS (Table 1). Each biofacies was named after the most dominant species with the highest factor loadings within each factor association. Biofacies abundance (%) was calculated based on cumulative percentages of all species contributing to that particular biofacies (Fig. 3). We have further classified and grouped these dominant 32 species into oxic, suboxic, and dysoxic species based on their environmental (oxygenation) preferences (Table 2).

The diversity among benthic foraminifera was calculated using the Shannon Index (H) (Shannon & Weaver, 1949), given by the formula:

$$H = - \sum_{i=1}^S p_i \ln p_i \quad (1)$$

where, S is the number of species in a given sample, p_i is the proportion of the i^{th} species in the sample, and \ln is the natural logarithm.

Spectral analysis was carried out using the PAST 4.03 program (Hammer et al., 2001) for the oxic genus *Quinqueloculina* (%), suboxic genus *Bulimina* (%), and dysoxic genus *Globobulimina* (%) and the productivity indicator $\delta^{13}\text{C}_{\text{pf}}$ (Clemens et al., 2018) over the investigated interval. We selected a ‘Welch’ window parameter to obtain the spectra at a 90 % confidence level (REDFIT). The spectrum was bias-corrected using the Monte Carlo simulation option (Schulz & Mudelsee, 2002).

183 Table 1. *Benthic Foraminiferal Biofacies, Factor Scores and their preferred Environments at Site*
 184 *U1429.*

Biofacies	Factor Scores	Environment	Age (ka)
1. Biofacies Gv (Factor 1 ^{-ve}) <i>Gavelinopsis</i> sp. <i>Oridorsalis umbonatus</i> <i>Gyrodinoides cibaoensis</i> <i>Quinqueloculina seminulum</i>	-0.64 -0.49 -0.46 -0.36	High energy conditions, pulsed food supply, oxic to slightly suboxic bottom water conditions	23-14
2. Biofacies Co (Factor 2 ^{+ve}) <i>Chilostomella oolina</i> <i>Fursenkoina rotundata</i> <i>Globobulimina pacifica</i>	0.81 0.52 0.36	High productivity, high food supply, highly dysoxic bottom water conditions	206, 93-41, and 27-17
3. Biofacies Hb (Factor 4 ^{+ve}) <i>Hyalinea balthica</i> <i>Bulimina mexicana</i> <i>Hoeglundina elegans</i> <i>Valvulineria sadonica</i>	-0.46 -0.44 -0.36 -0.32	Moderate to high influx of organic carbon, suboxic bottom water conditions	302-295, 39-30, and 15-0
4. Biofacies Ct (Factor 3 ^{+ve}) <i>Cassidulina teretis</i> <i>Epistominella exigua</i> <i>Cassidulina laevigata</i> <i>Bolivina robusta</i> <i>Globocassidulina subglobosa</i>	0.74 0.53 0.47 0.47 0.42	Enhanced but pulsed flux of phytodetritus, suboxic conditions with intermittent dysoxic conditions	331, 278-262, 153, 114-107, and 60-57
5. Biofacies Um (Factor 5 ^{-ve}) <i>Uvigerina mediterranea</i> <i>Uvigerina pygmaea</i> <i>Uvigerina peregrina</i>	-0.55 -0.49 -0.47	High productivity, high influx of organic matter, suboxic to slightly dysoxic bottom water conditions	390-386, 282-218, 188-138, and 29-1
6. Biofacies Mc (Factor 1 ^{+ve}) <i>Martinotiella communis</i> <i>Gaudryina</i> sp. <i>Amphicoryna scalaris</i> <i>Uvigerina auberiana</i> <i>Melonis barleeianum</i> <i>Bulimina aculeata</i>	0.44 0.41 0.33 0.33 0.32 0.32	Suboxic bottom water conditions, moderate organic carbon flux	396-283, 248-242, 212-193, 158, 135-122, 74 and 61

Table 2. *List of Oxic, Suboxic, and Dysoxic species recorded at Site U1429.*

Type:	Microhabitat	Species:
Oxic Species	Epifaunal	<i>Cibicidoides mundulus</i> (Kaiho, 1994; Pérez-Asensio et al., 2017)
	Epifaunal	<i>Cibicidoides wuellerstorfi</i> (Moumita Das et al., 2017; De & Gupta, 2010; Kaiho, 1994)
	Epifaunal	<i>Epistominella exigua</i> (Bhaumik et al., 2007; De & Gupta, 2010)
	Epifaunal	<i>Gavelinopsis</i> sp. (Akimoto & Hasegawa, 1989; Takata et al., 2018)
	Epifaunal	<i>Globocassidulina subglobosa</i> (Araújo et al., 2018; Kaiho, 1994; Kaminski, 2012; R. K. Singh et al., 2021; Verma et al., 2013)
	Epifaunal	<i>Quinqueloculina seminulum</i> (Moumita Das et al., 2017; Hayward et al., 1997; Kaminski, 2012; Laprida et al., 2007)
	Epifaunal	<i>Sigmoilopsis schlumbergeri</i> (Kaminski, 2012; Mackensen et al., 1995; Saravanan et al., 2019)
Suboxic Species	Shallow infaunal	<i>Amphicoryna scalaris</i> (García-Sanz et al., 2018; Kaminski, 2012)
	Intermediate to deep infaunal	<i>Bulimina aculeata</i> (Moumita Das et al., 2017; Kaiho, 1994; Kaminski, 2012)
	Deep infaunal	<i>Bulimina marginata</i> (Moumita Das et al., 2017; Kaminski, 2012; Saravanan et al., 2019)
	Infaunal	<i>Bulimina mexicana</i> (Grunert et al., 2018)
	Shallow infaunal	<i>Cassidulina laevigata</i> (Bubenshchikova et al., 2010; Schmiedl et al., 1997)
	Infaunal	<i>Cassidulina teretis</i> (Cronin et al., 2019; Mackensen & Hald, 1988)
	Shallow to deep infaunal	<i>Gaudryina</i> sp. (Rostami et al., 2020)
	Epifaunal	<i>Gyroidinoides cibaoensis</i> (Bhaumik et al., 2007; Moumita Das et al., 2017; De & Gupta, 2010)
	Epifaunal	<i>Hoeglundina elegans</i> (Gupta & Thomas, 1999; Kaiho, 1994, 1999; Sarkar & Gupta, 2014)
	Shallow infaunal	<i>Hyalinea balthica</i> (Charrieau et al., 2018; Moumita Das et al., 2017; Kaminski, 2012)
	Intermediate infaunal	<i>Melonis barleeianum</i> (Fontanier et al., 2002, 2005; Kaminski, 2012; Schmiedl et al., 2000)
	Infaunal	<i>Martinottiella communis</i> (Culver & Buzas, 1987; Jian et al., 1999; Kender & Kaminski, 2017)
	Infaunal	<i>Nonionina communis</i> (Diz & Francés, 2008; Fontanier et al., 2002)
	Shallow infaunal to epifaunal	<i>Oridorsalis umbonatus</i> (Bubenshchikova et al., 2010; Moumita Das et al., 2017)
	Infaunal	<i>Pullenia bulloides</i> (Moumita Das et al., 2017; Gupta & Thomas, 1999; Rathburn & Corliss, 1994)
	Infaunal	<i>Pullenia quinqueloba</i> (Moumita Das et al., 2017; Kaminski, 2012; N. Wang et al., 2018)
	Shallow infaunal	<i>Uvigerina auberiana</i> (Bubenshchikova et al., 2010; Gorbarenko et al., 2004; Kuhnt et al., 1999; Schmiedl et al., 1997)
	Shallow infaunal	<i>Uvigerina mediterranea</i> (Manisha Das et al., 2018; Schmiedl et al., 2000)
	Shallow infaunal	<i>Uvigerina peregrina</i> (Manisha Das et al., 2018; Lutze, 1979; Schmiedl et al., 1997; Schmiedl & Leuschner, 2005)
	Shallow infaunal	<i>Uvigerina pygmaea</i> (Manisha Das et al., 2018; Kastens & Mascle, 1990; Lutze, 1979)
	Intermediate infaunal	<i>Valvulineria sadonica</i> (Bubenshchikova et al., 2010)
Dysoxic Species	Infaunal	<i>Bolivina robusta</i> (Haller et al., 2018; Kaiho, 1994; B. Zhao et al., 2018)
	Deep infaunal	<i>Chilostomella oolina</i> (Kaiho, 1994; McGann & Conrad, 2018; N. Wang et al., 2018)
	Infaunal	<i>Fursenkoina rotundata</i> (Moumita Das et al., 2017; Kaiho, 1994; Patarroyo & Martínez, 2015)
	Deep infaunal	<i>Globobulimina pacifica</i> (Moumita Das et al., 2017; McGann & Conrad, 2018)

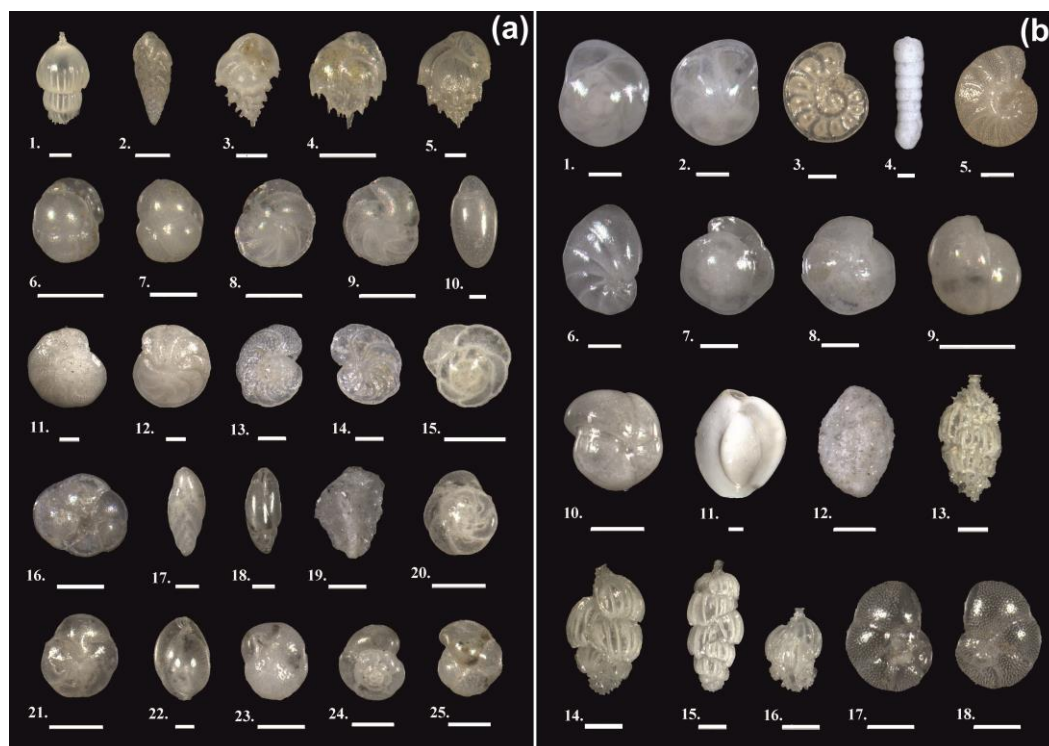


Figure 2. Light microscope photographs of the dominant benthic foraminifera (32 species) present at Site U1429. Plate (a): 1. *Amphicoryna scalaris* (side view) 2. *Bolivina robusta* (side view) 3. *Bulimina aculeata* (side view) 4. *Bulimina marginata* (side view) 5. *Bulimina mexicana* (side view) 6. *Cassidulina laevigata* (umbilical view) 7. *Cassidulina laevigata* (spiral view) 8. *Cassidulina teretis* (umbilical view) 9. *Cassidulina teretis* (spiral view) 10. *Chilostomella oolina* (side view) 11. *Cibicidoides mundulus* (spiral view) 12. *Cibicidoides mundulus* (umbilical view) 13. *Cibicidoides wuellerstorfi* (spiral view) 14. *Cibicidoides wuellerstorfi* (umbilical view) 15. *Epistominella exigua* (spiral view) 16. *Epistominella exigua* (umbilical view) 17. *Fursenkoina rotundata* (side view) 18. *Fursenkoina rotundata* (apertural view) 19. *Gaudryina* sp. (side view) 20. *Gavelinopsis* sp. (spiral view) 21. *Gavelinopsis* sp. (umbilical view) 22. *Globobulimina pacifica* (side view) 23. *Globocassidulina subglobosa* (apertural view) 24. *Gyroidinoides cibaoensis* (spiral view) 25. *Gyroidinoides cibaoensis* (umbilical view); Plate (b): 1. *Hoeglundina elegans* (spiral view) 2. *Hoeglundina elegans* (umbilical view) 3. *Hyalinea balthica* (spiral view) 4. *Martinottiella communis* (side view) 5. *Melonis barleenaum* (spiral view) 6. *Nonionina communis* (side view) 7. *Oridorsalis umbonatus* (spiral view) 8. *Oridorsalis umbonatus* (umbilical view) 9. *Pullenia bulloides* (side view) 10. *Pullenia quinqueloba* (side view) 11. *Quinqueloculina seminulum* (side view) 12. *Sigmoilopsis schlumbergeri* (side view) 13. *Uvigerina auberiana* (side

view) 14. *Uvigerina mediterranea* (side view) 15. *Uvigerina peregrina* (side view) 16. *Uvigerina*
pygmaea (side view) 18. *Valvulineria sadonica* (umbilical view) 19. *Valvulineria sadonica* (spiral
view) [All Scale bars = 100 μ m].

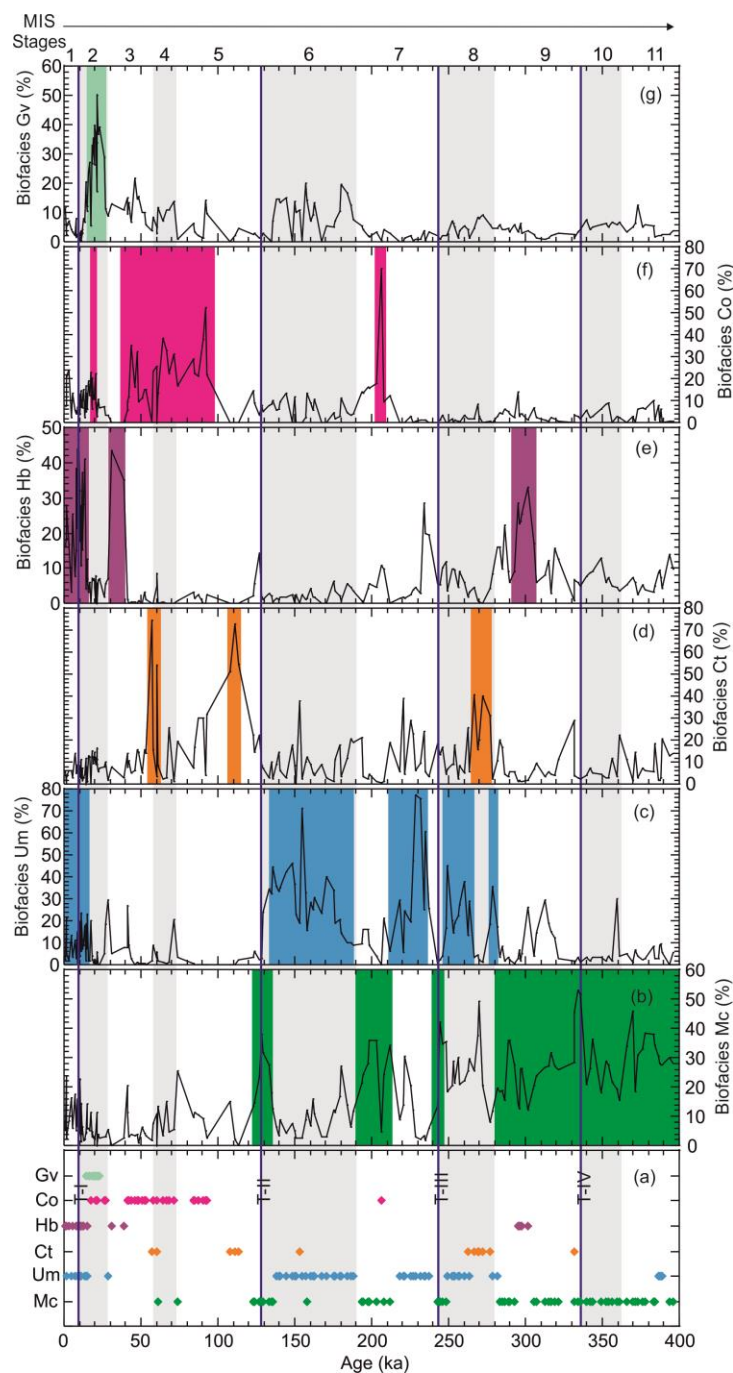


Figure 3. Benthic foraminiferal biofacies at Site U1429 plotted against interpolated ages (a-g), (a, b) Green shading and diamond indicate biofacies Mc (%), (a, c) Blue shading and diamond indicate biofacies Um (%), (a, d) Orange shading and diamond indicate biofacies Ct (%), (a, e) Purple

shading and diamond indicate biofacies Hb (%), (a, f) Pink shading and diamond indicate biofacies Co (%), (a, g) Light green shading and diamond indicate biofacies Gv (%). Mc- *Martinottiella communis*, Um- *Uvigerina mediterranea*, Ct- *Cassidulinia teretis*, Hb- *Hyalinea balthica*, Co- *Chilostomella oolina*, Gv- *Gavelinopsis* sp. Dark grey bars indicate MIS stages. Dark blue lines mark the termination events T-I, T-II, T-III, and T-IV.

4 Results

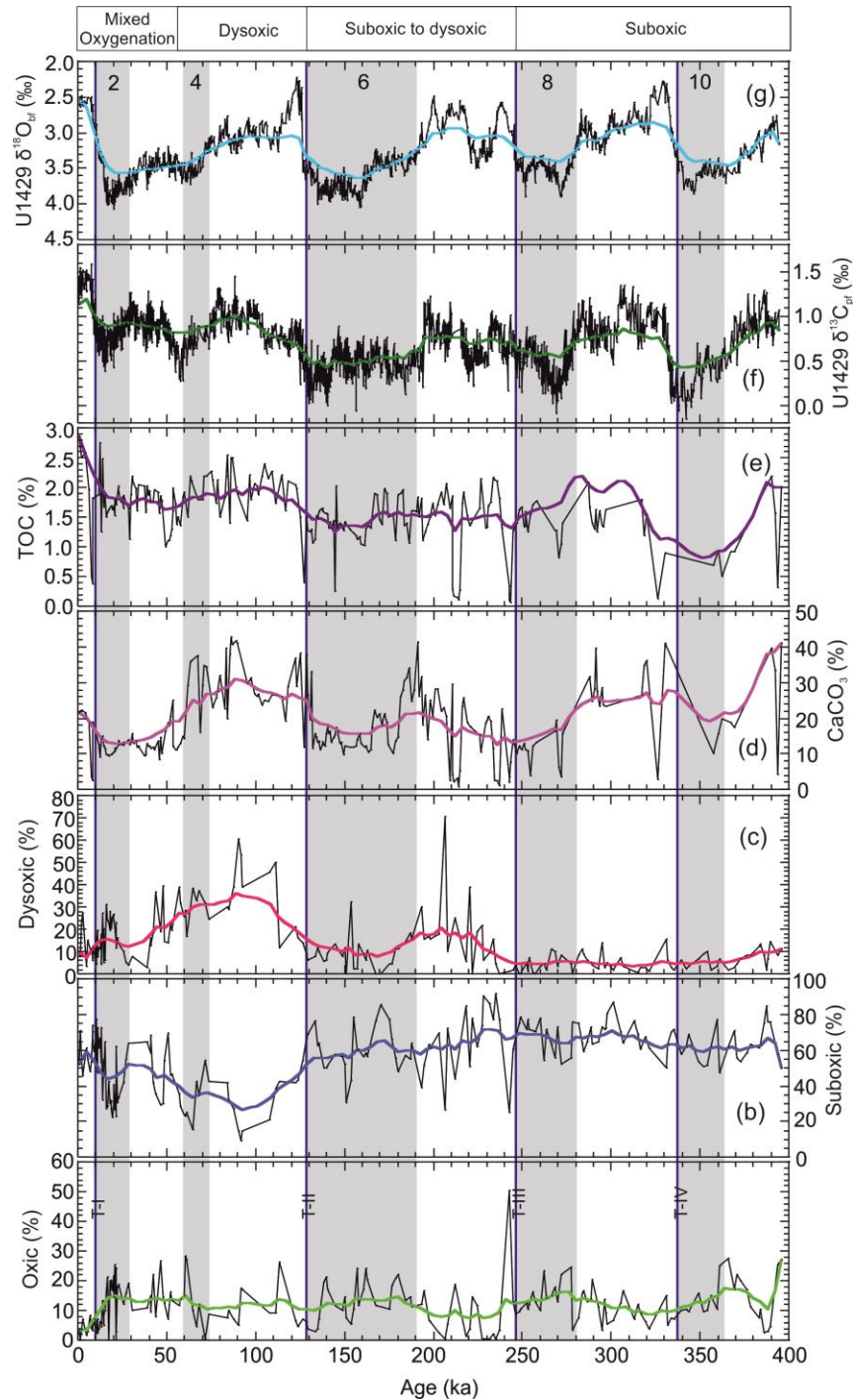
4.1 Temporal variability of oxic, suboxic and dysoxic species in the ECS

Following previous approaches, we use the term dysoxic, when dissolved oxygen (DO) is 0.1–0.3 mL/L, suboxic, when DO is 0.3–1.5 mL/L, and oxic, when DO is >1.5 mL/L (e.g., Gallagher et al., 2018; Kaiho, 1994; N. Wang et al., 2018). At Site U1429, most of the oxic species are epifaunal, the suboxic species are shallow to deep infaunal, and the dysoxic species are deep infaunal (Table 2). Since MIS 11 (~400 ka), oxic species were relatively less abundant in the ECS and did not show any significant variations in trends except for a peak just after T-III followed by intermittent occurrences during MIS 1 (Fig. 4). However, temporal variability of the dominant oxic genus *Quinqueloculina* has low abundance during certain peak abundance of oxic species (Fig. S3). Suboxic species were abundant between MIS 11 and 6, subsequently decreased during MIS 5 and 4, and increased once more in abundance between MIS 3 and 1 (Fig. 4). The temporal variation of the dominant suboxic genus *Bulimina* exhibits an overall similar trend, but displays higher variability (Fig. S3). Dysoxic species were relatively abundant during MIS 7 and 5, but abundance decreased between MIS 5 and 4, and they became relatively rare between MIS 3 and 2 (Fig. 4). The dominant dysoxic genus *Globobulimina* generally follows the same trend, but shows higher abundance during MIS 5 (Fig. S3).

4.2 Biofacies interpretation

For the identified six biofacies *Gavelinopsis* sp. (Gv), *Chilostomella oolina* (Co), *Hyalinea balthica* (Hb), *Cassidulinia teretis* (Ct), *Uvigerina mediterranea* (Um), and *Martinottiella*

237 *communis* (Mc) (Table 1), environmental significance is inferred, based on environmental
 238 preferences of individual species of that particular biofacies.



239

240 Figure 4. Plot of (a) Oxic species abundance (%), (b) Suboxic species abundance (%), (c) Dysoxic
 241 species abundance (%), (d) CaCO_3z (%) and (e) TOC (%) (Black et al., 2018); (f) Planktic

foraminiferal $\delta^{13}\text{C}_{\text{pf}}$ (‰) and (g) Benthic foraminiferal $\delta^{18}\text{O}_{\text{bf}}$ (Clemens et al., 2018) plotted against age at Site U1429. Dark blue lines mark the termination events T-I, T-II, T-III, and T-IV. The colored bold curves are smooth curve fit using Stineman function to the data and the output has a geometric weight applied to the current point and $\pm 10\%$ of the data range, applied using KaleidaGraph software. Dark grey bars indicate MIS stages.

4.2.1 Biofacies Gv

The biofacies Gv has high negative factor loading on Factor 1 and includes four species: *Gavelinopsis* sp., *Oridorsalis umbonatus*, *Gyroidinoides cibaoensis*, and *Quinqueloculina seminulum* (Table 1). This biofacies occurs almost continuously in 13 samples between 23 and 14 ka (Fig. 3). *Gavelinopsis* sp. is an epifaunal species found in the inner sublittoral zone of the Japanese coast (Akimoto & Hasegawa, 1989; Takata et al., 2018) and often inhabits high energy environments affected by wave and current processes (Takata et al., 2018). *Oridorsalis umbonatus* is a cosmopolitan species present over a range of water depths and trophic levels (Gupta et al., 2006; Schmiedl & Mackensen, 1997; R. K. Singh et al., 2021; Takata et al., 2019). It has also been reported as a suboxic and shallow infaunal to epifaunal species (Bubenshchikova et al., 2010; Jorissen et al., 1998). *Gyroidinoides cibaoensis* is found in a wider range of oxygen conditions with variable food availability (De & Gupta, 2010). *Quinqueloculina seminulum* is a cold-water dweller (Hayward et al., 1997), found in high-energy conditions (Laprida et al., 2007) with a pulsed food supply (Gupta & Thomas, 2003; Sarkar & Gupta, 2014; Takata et al., 2018), generally in shallow marine environments (Murray, 2006). Biofacies Gv overall indicates relatively high energy within an inner to outer shelf environment with a pulsed food supply and overall oxic to slightly suboxic bottom water conditions.

4.2.2 Biofacies Co

Biofacies Co is defined by the species having high positive factor loadings on Factor 2 (Table 1). *Chilostomella oolina*, *Fursenkoina rotundata*, and *Globobulimina pacifica* are characteristic of this biofacies. This biofacies occurs in 29 samples, almost continuously between ~93 and 41 ka and occasionally at other times (Fig. 3). *Chilostomella oolina* is a deep infaunal species typifying dysoxic conditions (Jorissen et al., 1998; McGann & Conrad, 2018) with high productivity (N. Wang et al., 2018). *Fursenkoina rotundata* is an infaunal, dysoxic, opportunist

species (Moumita Das et al., 2017), present in areas where there is significant organic matter influx associated with high surface productivity leading to low-oxygen conditions (Patarroyo & Martínez, 2015). *Globobulimina pacifica* is also a low oxygen tolerant taxon (Ballesteros-Prada, 2019; Bernhard et al., 1997; McGann & Conrad, 2018). It occupies intermediate to deep-infaunal microhabitats in dysoxic conditions (Moumita Das et al., 2017) and is commonly associated with poorly ventilated deep-water (Ma et al., 2019). Biofacies Co indicates strongly dysoxic bottom water conditions in the ECS associated with high productivity.

4.2.3 Biofacies Hb

Biofacies Hb has high negative factor loadings on Factor 4 (Table 1). *Hyalinea balthica*, *Bulimina mexicana*, *Hoeglundina elegans*, and *Valvulineria sadonica* are characteristic species of this biofacies. This biofacies is present in 22 samples at ~302-295, ~39-30 and ~15-0 ka (Fig. 3). *Hyalinea balthica* is a shallow infaunal, opportunistic species present in food-abundant regions with suboxic conditions (Charrieau et al., 2018; Moumita Das et al., 2017). *Bulimina mexicana* is a cosmopolitan taxon that thrives in intermediate (bathyal) water depths in all ocean basins (Culver & Buzas, 1980; Grunert et al., 2018; Jones & Brady, 1994; Van Morkhoven et al., 1986). It generally prefers a shallow infaunal microhabitat, high fluxes of organic matter and oxygen-depleted sediments (Grunert et al., 2018). *Hoeglundina elegans* is a shallow infaunal taxon (Gonzales et al., 2017; Jorissen et al., 1998) and was reported in the upwelling zones of the Bay of Biscay (Martínez-García et al., 2013). The species is present in moderately oxygen-depleted environments in the Arabian Sea and is considered as suboxic species (Gupta & Thomas, 1999; Kaiho, 1994, 1999; Sarkar & Gupta, 2014). *Valvulineria sadonica* is found in areas with a high flux of degraded and refractory organic matter in shallow subsurface water (Gorbarenko et al., 2010; Phleger & Soutar, 1973; Smith, 1964). It is an intermediate infaunal species typifying mostly suboxic conditions and within the Oxygen Minimum Zone (OMZ) in the Okhotsk Sea (Bubenshchikova et al., 2010). Biofacies Hb suggests a high influx of organic matter and overall suboxic bottom water conditions.

4.2.4 Biofacies Ct

Biofacies Ct is characterized by five species *Cassidulina teretis*, *Epistominella exigua*, *Cassidulina laevigata*, *Bolivina robusta*, and *Globocassidulina subglobosa* with positive high

factor loadings on Factor 3 (Table 1). This biofacies occurs sporadically in 13 samples during 278-262, ~153, 114-107, ~60 and ~57 ka (Fig. 3). *Cassidulina teretis* is a common high latitude species present in the cold Arctic Ocean and off Alaska (Cronin et al., 2019; Mackensen & Hald, 1988). This species typifies seasonally ice-free regions and is associated with high productivity and high phytodetritus influx (Cronin et al., 2019; Scott et al., 2008). *Epistominella exigua* is a cosmopolitan species feeding opportunistically on phytodetritus deposited seasonally on the seafloor and can tolerate a varying organic export flux (Manisha Das et al., 2021; Gooday, 1988; R. K. Singh & Gupta, 2004, 2010). *Cassidulina laevigata*, is a shallow infaunal taxon (Fontanier et al., 2002), typifying relatively cold waters with high organic matter content (Pascual et al., 2020), and is tolerant of moderate oxygen depletion in bottom and pore water under high organic flux rates (Manisha Das et al., 2021; Nardelli et al., 2014; Sen Gupta & Machain-Castillo, 1993). *Bolivina robusta* is an open ocean infaunal species found in temperate to subtropical middle to upper bathyal depths (Haller et al., 2018; B. Zhao et al., 2018). *Bolivina robusta* may be able to tolerate high eutrophication and is a useful indicator of low oxygen condition at the seafloor (B. Zhao et al., 2018). *Globocassidulina subglobosa*, which prefers oxic conditions and high to intermediate food supply, is a cosmopolitan epifaunal species (Araújo et al., 2018; Manisha Das et al., 2021; Kaminski, 2012; Martins et al., 2007; Murray, 2006; R. K. Singh et al., 2021; Verma et al., 2013). Biofacies Ct indicates an enhanced phytodetritus flux into the ECS associated with suboxic conditions that occasionally become dysoxic, as shown by the presence of *B. robusta*.

4.2.5 Biofacies Um

Biofacies Um has high negative factor loadings on Factor 5 (Table 1). It is comprised of *Uvigerina mediterranea*, *Uvigerina pygmaea*, and *Uvigerina peregrina*. This biofacies is present during 55 samples at ~390-386, ~282-218, 188-138, and ~29-1 ka (Fig. 3). *Uvigerina mediterranea* is a low to intermediate oxygen tolerant shallow infaunal species of middle to lower bathyal depths (Manisha Das et al., 2018, 2021; Duros et al., 2011; Schmiedl et al., 2000; Schweizer, 2006; A. D. Singh et al., 2015). *Uvigerina pygmaea* is also a shallow infaunal species, typical of intermediate to low oxygen environments in deep-water masses (Kastens & Mascle, 1990; Lutze, 1979). The environmental preferences of *Uvigerina pygmaea* are similar to that of *Uvigerina peregrina* (Manisha Das et al., 2018). *Uvigerina peregrina* is a shallow infaunal species (Jorissen et al., 1998) typical of middle neritic to lower bathyal depths (Schweizer, 2006). It is

often associated with high productivity and sustained flux of organic matter and can tolerate lower food levels and oxygen deficiency (Manisha Das et al., 2018, 2021; Moumita Das et al., 2017; Gupta et al., 2008; Mazumder & Nigam, 2014). Biofacies Um suggests suboxic to dysoxic bottom water conditions in the ECS with a relatively higher influx of organic matter.

4.2.6 Biofacies Mc

Biofacies Mc has high positive factor loadings on Factor 1 (Table 1) and is characterized by two agglutinated species: *Martinottiella communis* and *Gaudryina* sp. along with the calcareous species *Amphicoryna scalaris*, *Melonis barleeaanum*, *Uvigerina auberiana*, and *Bulimina aculeata*. It is present in 57 samples during ~396-283, ~248-242, ~212-193, ~158, ~135-122, 74 and ~61 ka (Fig. 3). *Martinottiella communis* is an agglutinated foraminifera, often found in shelf to bathyal conditions (Kaiho & Nishimura, 1992). It may be present in regions with a high organic carbon flux and is tolerant of moderate to low oxygen settings (Kender & Kaminski, 2017). It is found within a DO range 4.7 to 5.7 mL/L in the Scotia Sea and Argentine Basin (Harloff & Mackensen, 1997). *Gaudryina* sp. is also an agglutinated species that has a shallow to deep infaunal habitat (Reolid et al., 2012). It has been reported as an endobenthic species associated with moderately oxygenated environments (Rostami et al., 2020). *Amphicoryna scalaris* is a shallow infaunal species (Balestra et al., 2017), associated with a high input of labile organic matter (Fontanier et al., 2008), and has been reported in moderately oxygenated environments (García-Sanz et al., 2018). *Melonis barleeaanum* is often associated with degraded refractory organic matter, and is an infaunal species found in moderately oxygen-depleted condition (Fontanier et al., 2002, 2005; Schmiedl et al., 2000). The shallow infaunal *Uvigerina auberiana*, reported as a suboxic species in the Okhotsk Sea (Bubenshchikova et al., 2010; Gorbarenko et al., 2004), prefers a higher organic carbon flux and has also been reported in the South China Sea (Kuhnt et al., 1999). *Bulimina aculeata* is an intermediate to deep infaunal taxon, mostly abundant in suboxic bottom water conditions (Moumita Das et al., 2017; Kaiho, 1994; Kaminski, 2012). Biofacies Mc suggests suboxic bottom water conditions in the ECS with moderate organic export flux.

4.3 Temporal variability of marine productivity indicators in the ECS

Marine productivity indicators such as CaCO_3 (%), TOC (%) (Black et al., 2018), and $\delta^{13}\text{C}_{\text{Pf}}$ (‰) (Clemens et al., 2018) are used to complement the benthic foraminiferal distribution

data. CaCO_3 (%) was relatively high (41.17 %) during mid-MIS 11, but gradually decreased to 10.13 % during MIS 10 (Fig. 4). CaCO_3 (%), increased again during MIS 9 with an average of 28.24 %, then decreased to its lowest value of 3.65 % during MIS 8 with an average value of 11.51 % during this interval. CaCO_3 (%) continued to be relatively low (average value 16.66 %) during MIS 7 and 6 (Fig. 4) before increasing to its highest value (42.84 %) during MIS 5 (average 29.76 %), then gradually decreased to modern-day values (21.54 %) after MIS 5 (Fig. 4). The TOC (%) trend at Site U1429 is comparable to that of CaCO_3 (%) between MIS 11 and MIS 8 with values between 2.2 % and 0.13 % (average 1.33 %), followed by small variations between 2.17 % and 0.77 % (average 1.39 %) until MIS 6 (Fig. 4). TOC (Wt %) increased between MIS 5 and 1, and reached a maximum value of 2.85 % during MIS 1 (Fig. 4). The $\delta^{13}\text{C}_{\text{pf}}$ (‰) values exhibit a decreasing trend toward MIS 10, ranging between 1.29 and 0.3 ‰ (VPDB), then gradually declined to -0.15 ‰ during MIS 10. During MIS 9, $\delta^{13}\text{C}_{\text{pf}}$ (‰) increased to 1.35 ‰, then declined to -0.08 ‰ during MIS 8. The $\delta^{13}\text{C}_{\text{pf}}$ (‰) values ranged between -0.06 ‰ to 1.22 ‰ during MIS 7 and MIS 6 with an average of 0.55 ‰ before increasing to 1.44 ‰ during MIS 5 and later declining during MIS 2. $\delta^{13}\text{C}_{\text{pf}}$ (‰) increased to 1.58 ‰ during MIS 1. Overall, the $\delta^{13}\text{C}_{\text{pf}}$ (‰) values exhibit a declining trend during all glacial intervals (MIS 2, 4, 6, 8 and 10) (Figs. 4, 5).

4.4 Spectral analysis

Spectral analysis of oxic genus *Quinqueloculina* (%) shows prominent cyclicity of 106, 23, 7, and 6 kyr (Fig. 6a). The suboxic genus *Bulimina* (%) shows abundance peaks at 44, 23, 13, 11, 10, 5, and 4 kyr (Fig. 6b) and the dysoxic genus *Globobulimina* (%) at 132, 24, 8, 7, and 6 kyr (Fig. 6c). The spectral analysis of $\delta^{13}\text{C}_{\text{pf}}$ exhibits peaks at 105, 40, 28, 23 kyr (Fig. 6d).

5 Discussion

5.1 ECS Bottom water oxygenation history

5.1.1 MIS 11 to MIS 8

The ECS bottom water remained overall suboxic between MIS 11 and 8, as shown by the consistent occurrences of the suboxic biofacies Mc, Ct and Hb (Fig. 3). Suboxic bottom water conditions at the sediment-water interface in the ECS during MIS 11 to 8 are supported by the dominance of suboxic species and the lower abundance of dysoxic species (Fig. 4). The water

column above the sediment-water interface may have remained oxic, as evidenced by the abundance of the oxic radiolarian species *C. davisiana* (Matsuzaki et al., 2019). No major benthic foraminiferal turnover occurred during this phase, as suggested by relatively constant benthic foraminiferal diversity (Fig. 5).

5.1.2 MIS 7 to MIS 6

Towards the end of MIS 8, bottom water became suboxic to dysoxic, as indicated by a small decline in suboxic species and an increasing trend of dysoxic species (Fig. 4). The ECS bottom water was overall suboxic to dysoxic during MIS 7 (Biofacies Um; Figs. 3, 5), except for some transient moderate productivity events characterized by intermittent increases in the suboxic biofacies Mc (Fig. 3). The overall diversity was low during this period and the abundance of dysoxic species was relatively high (Figs. 4, 5). These suboxic to dysoxic conditions continued during MIS 6, as suggested by the dominance of biofacies Um (Figs. 3, 5).

5.1.3 MIS 5 to MIS 4

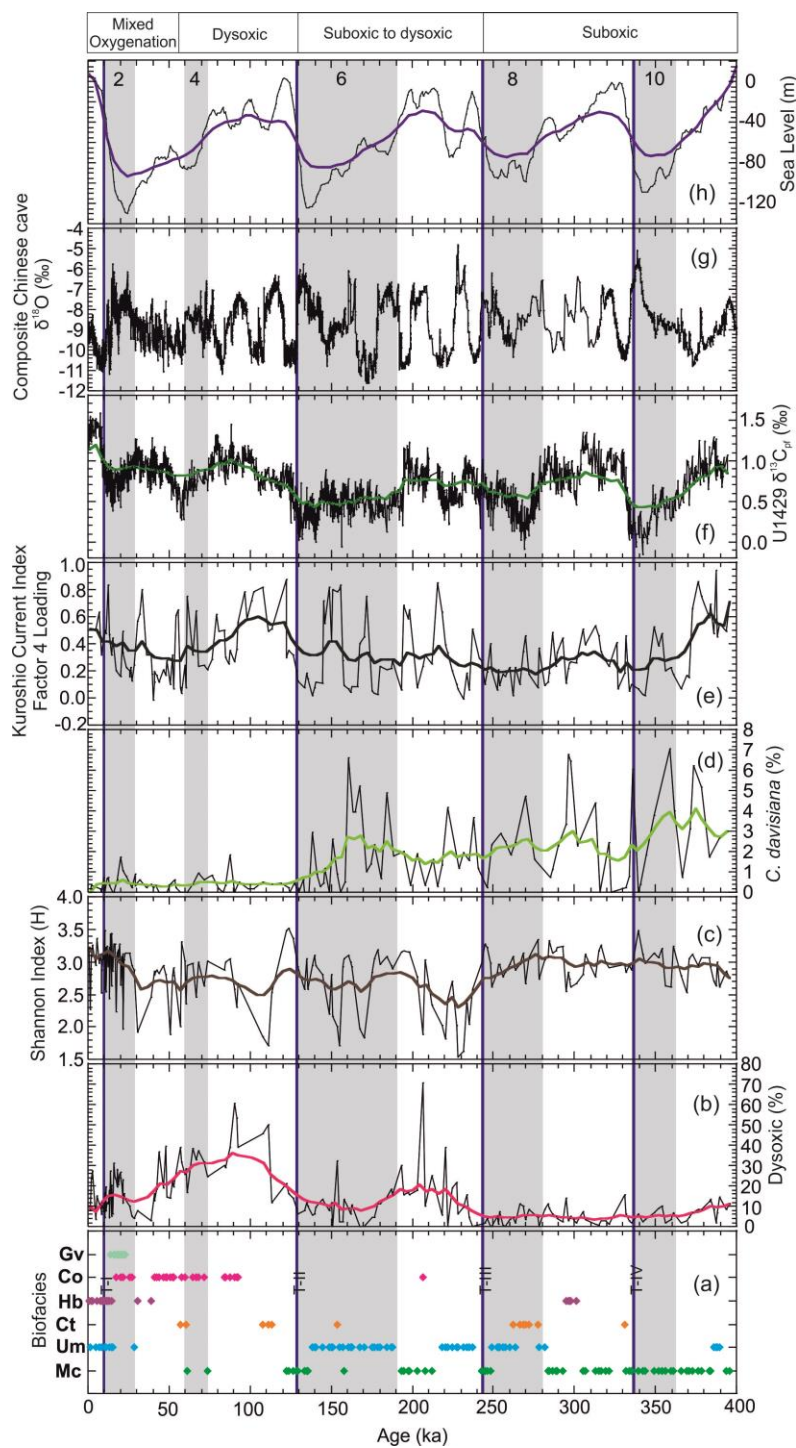
The ECS bottom water was suboxic during MIS 5 with intermittent dysoxic pulses (biofacies Mc and Ct; Figs. 3, 5) between T-II and ~110 ka. The occurrence of biofacies Ct during MIS 5 indicates enhanced pulsed phytodetritus input in the ECS. Nevertheless, dysoxic conditions prevailed from mid-MIS 5 (~110 ka) to MIS 4, which is evident from the abundance of the dysoxic species, *Globobulimina* genus and biofacies Co (Figs. 3, 5; Fig. S3). During the termination event, T-II, a major switch in deep-sea oxygenation occurred at the sediment/water interface as well as within the water column, which corresponds to a decrease in the oxic radiolarian species *C. davisiana* (Matsuzaki et al., 2019). The end of the glacial MIS 4 coincided with an improvement in bottom water oxygenation in the ECS, marked by the occurrence of biofacies Ct (Fig. 3). The marine productivity indicators and the dysoxic species exhibited declining trends, whereas the suboxic species displayed an increasing trend, which together suggests that productivity decreased by the end of MIS 4 (Fig. 4).

5.1.4 MIS 3 to MIS 1

Bottom water conditions in the ECS were characterized by variable oxygen concentrations between MIS 3 and 1, as shown by the occurrence of biofacies Um, Hb, Co and Gv (Figs. 3, 5). An increase in suboxic species abundance suggests the prevalence of suboxic as well as intermittent dysoxic conditions during MIS 3. The ECS water became oxic during the glacial MIS 2, as indicated by the occurrence of biofacies Gv and a slightly increasing trend of oxic species coincident with a declining trend of suboxic species (Figs. 3, 4, 5). The alternations between biofacies Hb and Um and the shifts in the abundance of suboxic species (Figs. 3, 4, 5) during MIS 1 suggest variable bottom water oxygenation.

5.2 Kuroshio Current as a forcing factor of ECS bottom water oxygenation

The KC intrusion onto the ECS shelf was stronger during interglacial periods (Vats et al., 2021; MIS 11, 9, 7, and 5), whereas the lowering of sea level adversely influenced KC intrusion in the ECS. For instance, a 43 % reduction in KC inflow occurred during the LGM linked to the sea-level low stand (Kao et al., 2006). The upwelling of subsurface KC, a major nutrient supplier in the ECS (Chen et al., 1995; K. K. Liu et al., 1992; Vats et al., 2020; Wu et al., 2008; P. Zhou et al., 2018b), significantly increases primary productivity in the upper layer, leading to the sinking of organic matter to sea floor. In addition, the shallow nature of the ECS and its trough-like bathymetry promote the sinking of organic matter. During interglacial periods (MIS 11, 9, 7, and 5), rapid utilization of dissolved oxygen by sinking organic matter in the ECS water column caused suboxic to dysoxic bottom water conditions, which varied in relation to the intensity of KC upwelling. Furthermore, EASM precipitation was high during interglacial periods and ECS bottom water oxygenation was affected by both EASM and KC. By contrast, KC intrusion was low during glacial periods (10, 8, 6, and 2), when sea level was relatively low (Vats et al., 2020; Spratt & Lisiecki, 2016; Fig. 5), and EASM precipitation played a major role in controlling primary productivity during glacial periods.



437

438 Figure 5. (a) Benthic foraminiferal biofacies, (b) Dysoxic species abundance (%), (c) Benthic
 439 foraminiferal diversity as Shannon Index (H), (d) Oxidic radiolarian species *C. davisiana* (%)
 440 (Matsuzaki et al., 2019), (e) KC Index- Factor 4 loading (Vats et al., 2020), (f) $\delta^{13}C_{pf}$ (‰) (Clemens
 441 et al., 2018) at Site U1429, and (g) Composite Chinese cave $\delta^{18}O$ (‰) as Asian Monsoon indicator

(Cheng et al., 2016) and (h) Late Pleistocene Sea level stack (Spratt & Lisiecki, 2016). Dark blue lines mark termination events T-I, T-II, T-III, and T-IV. The colored bold curves are smooth curve fit using Stineman function to the data and the output has a geometric weight applied to the current point and $\pm 10\%$ of the data range, applied using KaleidaGraph software. Dark grey bars indicate MIS stages.

5.3 East Asian Summer Monsoon as a forcing factor of ECS bottom water oxygenation

The EASM influences the ECS bottom water oxygenation by supplying massive terrigenous (refractory) organic matter and/or nutrients (Lee et al., 2001; Matsuzaki et al., 2016). The Yangtze River estuaries exhibit summertime hypoxia due to increased primary productivity, which may extend from the continental shelf area to the OT (D. Li et al., 2002; Wei et al., 2007; Zhu et al., 2011).

During MIS 10, the EASM was relatively weak, as suggested by the composite $\delta^{18}\text{O}$ values from the Sanbao cave (Cheng et al., 2016; Clemens et al., 2018; Fig. 5), and productivity was low (lighter $\delta^{13}\text{C}_{\text{pf}}$, low TOC (%) and low CaCO_3) in the ECS (Fig. 4). A weak monsoon reduced the terrigenous organic matter flux leading to lower mass accumulation rates (Anderson et al., 2018) and to lower TOC (%) and CaCO_3 (%) (Black et al., 2018; Fig. 4). The weak EASM and KC acted in concert to reduce the total amount of organic carbon sinking to the bottom of the ECS during MIS 10, resulting in an oxic to suboxic water column, as indicated by the abundance of the oxic radiolarian species *C. davisiana* (Fig. 5; Matsuzaki et al., 2019) and the foraminiferal suboxic genus *Bulimina* and oxic genus *Quinqueloculina* (Fig. S3). During MIS 9, SST increased in the ECS and EASM precipitation became enhanced (Clemens et al., 2018; Vats et al., 2020), leading to a higher CDW discharge (Vats et al., 2020) and to suboxic bottom water conditions that became dysoxic by the end of MIS 8 during termination T-III (biofacies Um; Figs. 3, 5). The prevalence of warm conditions is also supported by higher abundances of the shallow warm water radiolarian genus *Tetrapyle* (Matsuzaki et al., 2019) and planktic foraminifera *Globigerinoides ruber* (Vats et al., 2020).

The strengthening of the EASM and KC during MIS 7 maintained higher productivity in the ECS. By contrast, the KC was relatively weaker during MIS 6, as suggested by the declining trend of the KC indicator species *Globigerinoides ruber* (Vats et al., 2020), and SST varied within

a range of $\pm 1^\circ\text{C}$ in the ECS (Clemens et al., 2018). Warm ECS condition, also supported by the presence of the planktic foraminifera *Globorotalia inflata* at the end of MIS 6 (Vats et al., 2020) may have been associated with changes in Northern Hemisphere insolation (Pahnke, 2003). These warmer conditions enhanced EASM precipitation, while the sea level low stand exposed most of the ECS continental shelf, leading to a shift of the Yellow/Yangtze River estuaries towards the OT (Ijiri et al., 2005; Kawahata & Ohshima, 2004; Tada et al., 2015; Xie et al., 1995; D. Zhao et al., 2017). The increased EASM precipitation and shift of the river mouths enhanced the input of terrigenous organic matter to the OT, as indicated by the prevalence of the suboxic to dysoxic biofacies Um (Figs. 3, 5). The relatively stable TOC (%) synchronous with a CaCO_3 (%) decline also confirms that the terrigenous organic export flux increased in relation to primary productivity. The development of oxygen depleted conditions in the OT bottom waters during MIS 6 was comparable to modern-day formation of hypoxia in river estuaries of the ECS.

The enhanced pulsed phytodetritus input (biofacies Ct during MIS 5 onset; Figs. 3, 5) may have been linked to the strengthening of the KC and EASM during MIS 5 (Cheng et al., 2016; Clemens et al., 2018; Vats et al., 2020) in the ECS. Further strengthening of the KC and EASM induced rapid sinking of organic matter and consumption of dissolved oxygen from the entire water column during MIS 5; ultimately leading to dysoxic bottom water conditions in the ECS that continued during MIS 4. CaCO_3 (%), TOC (%), and $\delta^{13}\text{C}_{\text{pf}}$ (‰) values suggest higher productivity associated either with upwelling of the subsurface KC and/or increased influx from the CDW discharge (Vats et al., 2020; Matsuzaki et al., 2019).

Although the KC was generally weak during MIS 3-2, enhanced EASM (Vats et al., 2020) may have caused suboxic and intermittent dysoxic conditions in the ECS. The relatively stable trend of TOC values and $\delta^{13}\text{C}_{\text{pf}}$ values during MIS 3-2 indicates that primary productivity remained high, suggesting a higher influx of terrigenous organic matter and nutrients delivered by the CDW (Vats et al., 2020). However, during the LGM, sea level fell by ~ 120 m and EASM precipitation intensity weakened (Jiang & Lang, 2010; Sun et al., 2021). Together these conditions led to a substantial decline in marine productivity (lighter $\delta^{13}\text{C}_{\text{pf}}$ (‰) and low CaCO_3 (%); Fig. 4) and prevalence of oxic bottom water conditions in the ECS (Anderson et al., 2018; Kubota et al., 2010). The interplay of biofacies Um and Hb during MIS 1 (Figs. 3, 5) suggests variable bottom water oxygenation, related either to the variability of EASM precipitation or the KC strength. Higher-

501 resolution studies are required to further constrain the variability of ECS deep-water oxygenation
502 on millennial to centennial-scales over the last two MIS stages.

503 5.4 Evolution of productivity and bottom water oxygenation in the ECS in relation to global 504 climate trends

505 Benthic foraminiferal proxy data indicate marked variability in productivity, organic
506 export flux and bottom water oxygenation over the last 400,000 years in the ECS. The oxic genus
507 *Quinqueloculina* (%), and the productivity indicators $\delta^{13}\text{C}_{\text{pf}}$ exhibits ~100 kyr cyclicity (Fig. 6).
508 Clemens et al. (2018) suggested that glacial-interglacial climate variability exerted an important
509 control on local seawater properties (i.e., riverine influx). Thus, the 100 kyr cyclicity signal in
510 *Quinqueloculina* (%) and the productivity indicator $\delta^{13}\text{C}_{\text{pf}}$ (Figs. 6a, 6d) is in phase with the 100
511 kyr cyclicity in local $\delta^{18}\text{O}_{\text{sea water}}$ in the EASM run-off (Clemens et al., 2018) in the ECS. The Asian
512 monsoon precipitation is modulated by global ice volume and greenhouse gases 100 kyr cyclicity
513 during the middle to late Pleistocene (Clemens et al., 2021). Therefore, the long-term variations
514 oxygenation of ECS bottom water was likely influenced by EASM related primary productivity
515 changes linked to variations in nutrient input derived from terrestrial organic matter in the ECS;
516 which may have been associated with greenhouse forcing or high-latitude ice sheet forcing during
517 the late Pleistocene (Clemens et al., 2018, 2021).

518 Glacial-interglacial seas level changes additionally controlled the intensity of the KC
519 intensity and the Tsushima warm current into the Japan Sea (Das et al., 2018, 2020; Gallagher et
520 al., 2018; Saavedra-Pellitero et al., 2019). Spectral analysis of the oxic genus *Quinqueloculina*
521 (%), suboxic genus *Bulimina* (%), dysoxic genus *Globobulimina* (%) and productivity indicator
522 $\delta^{13}\text{C}_{\text{pf}}$ additionally reveals a prominent ~23 kyr cyclicity, likely related to KC-driven productivity
523 changes in the ECS. Precession exerts a strong control on the KC inflow and the associated
524 Tsushima Warm Current in the neighbouring Japan Sea (Vats et al., 2020, Das et al., 2021), which
525 in turn strongly influences productivity and bottom water oxygenation in the ECS. The
526 strengthening of KC in La Niña conditions (J. Wang et al., 2020) and dominance of 23 kyr
527 precession scale variance in benthic foraminiferal proxy records suggests that enhanced summer

insolation forcing plays more important role in controlling the bottom water oxygenation of the ECS than the associated long-term variations in the bottom water oxygenation.

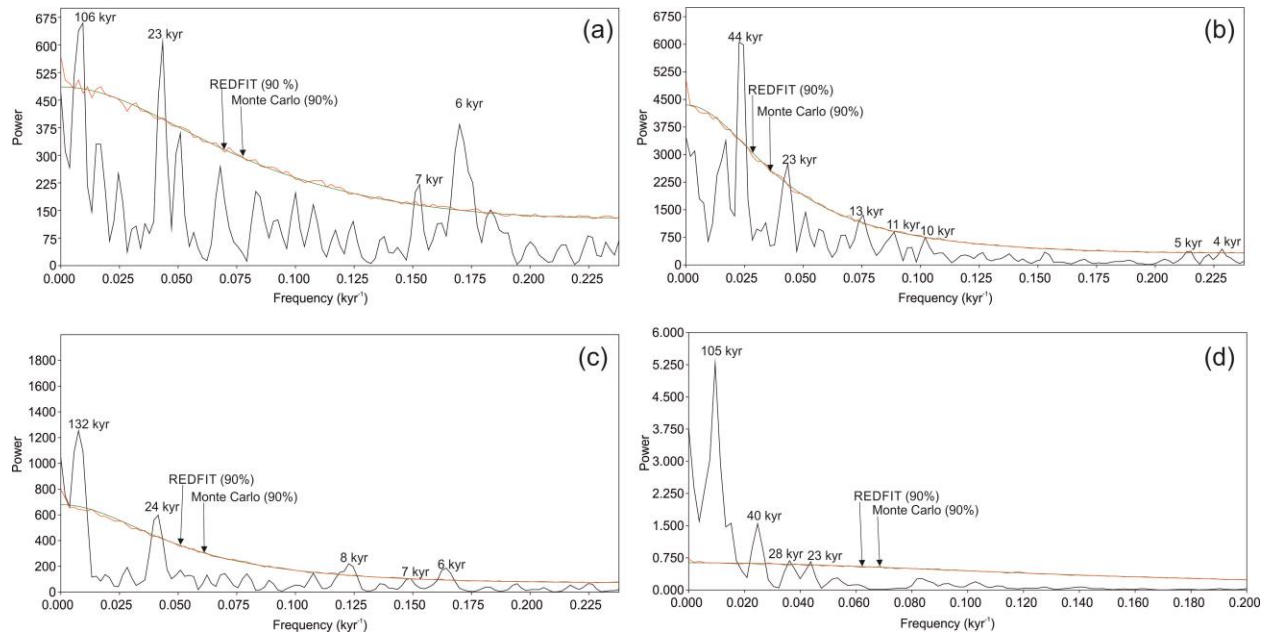


Figure 6. Spectral analysis of (a) oxic genus *Quinqueloculina* (%), (b) suboxic genus *Bulimina* (%), (c) dysoxic genus *Globobulimina* (%), and (d) $\delta^{13}\text{C}_{\text{pf}}$ (‰) at Site U1429 for the period 400 to 0 ka revealing significant periodicities at 90% significance level.

Thus, in summary, we observe that stronger KC often accompanied with Stronger EASM (e.g., during MIS 5) deposits massive organic matter and forms dysoxic bottom water conditions in the ECS. Relative strengthening of either KC or EASM (e.g., during MIS 7 and 6 respectively) causes suboxic to dysoxic bottom water conditions. However, strengthening of KC (e.g., during MIS 11 and 9) and weaker EASM (e.g., during MIS 10 and 8) cause suboxic bottom water conditions in the ECS. The simultaneous weakening of KC and EASM (e.g., during LGM) can cause oxic bottom water conditions in the ECS. The overall forcing mechanism of the bottom water oxygenation during different phases over the last 400 ka in the ECS is summarized in Fig. 7.

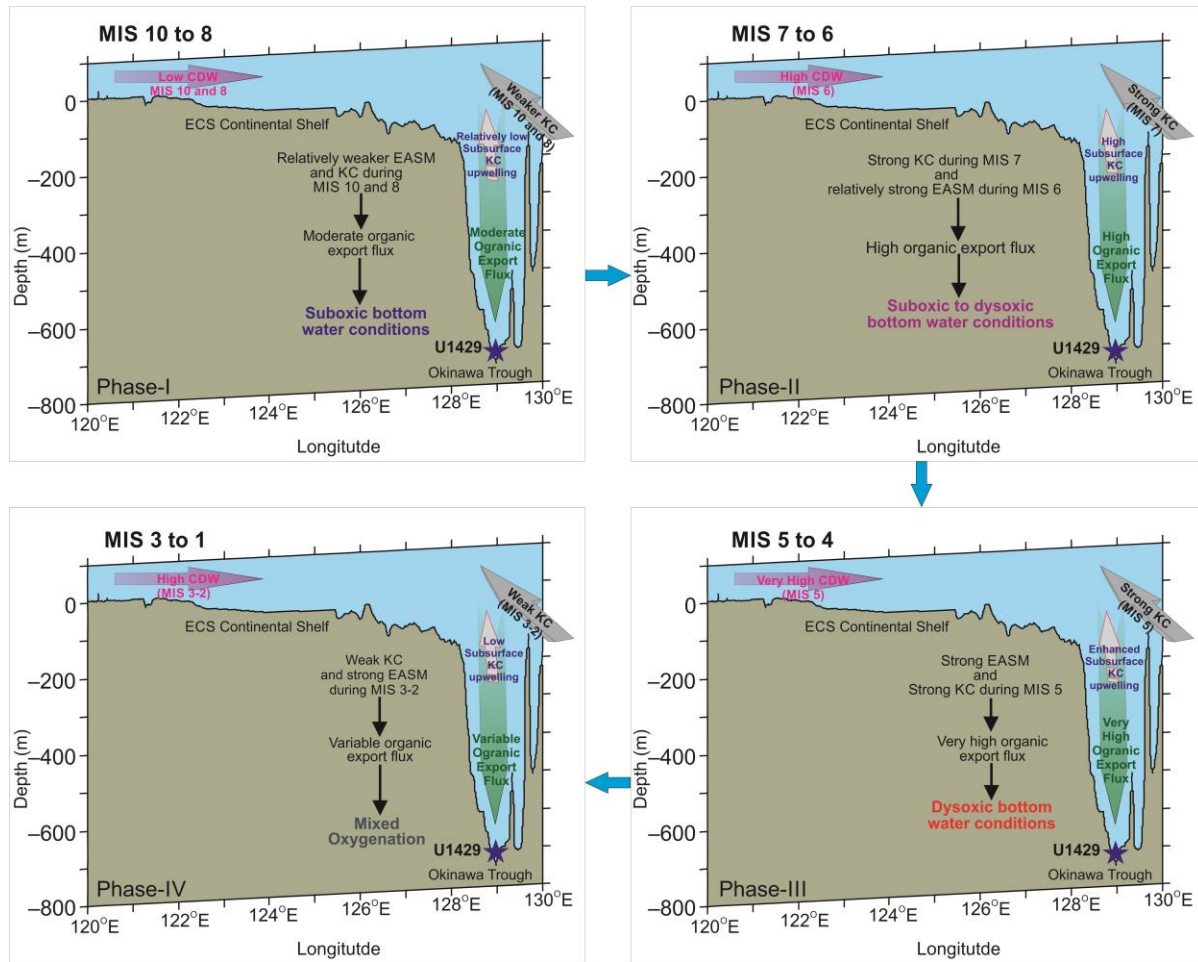


Figure 7. Schematic representation of forcing mechanisms controlling bottom water oxygenation over the last ~400 ka in the ECS.

6 Conclusions

Multivariate analysis of benthic foraminiferal assemblages allows retracing of the history and variability in ECS bottom water oxygenation over the last 400 kyr, suggesting four different phases of bottom water oxygenation. Bottom water was generally suboxic between mid MIS 11 and the end of MIS 8, except for transient intervals of suboxic to dysoxic conditions during MIS 8. The ECS bottom water subsequently became suboxic to dysoxic during MIS 7 and 6, reflecting a general increase in productivity, then remained dysoxic during MIS 5 and 4. Bottom water oxygenation exhibited major changes between oxic to dysoxic conditions from MIS 3 to 1. The dominant biofacies in the ECS over the last 400 kyr are biofacies Mc representing suboxic condition, biofacies Um representing suboxic to dysoxic condition and biofacies Co representing

dysoxic conditions. The oxic benthic foraminifera and marine productivity proxy $\delta^{13}\text{C}_{\text{pf}}$ respond to the global ice volume change and greenhouse gas modulated 100 kyr East Asian Monsoon precipitation cycle. The oxic, suboxic, and dysoxic foraminiferal genera and marine productivity proxy $\delta^{13}\text{C}_{\text{pf}}$ respond to 23 kyr precessional variability related to changes in the EASM and KC strength. This study suggests that bottom water oxygenation in the ECS is directly influenced by primary marine productivity and by the terrigenous supply of organic matter on 100 and 23 kyr time scales.

Data Availability Statement

Benthic foraminiferal percentage abundance data for last 400 kyr from Site U1429 generated for this study. Major benthic foraminiferal abundance data, Biofacies abundance data and oxic-suboxic-dysoxic benthic foraminiferal species abundance data archived at Mendeley Data (<http://dx.doi.org/10.17632/gcsgc2byps.1>; Vats et al., 2021, with closed access until acceptance).

Acknowledgments

The authors are grateful to IODP for providing core samples to RKS (Request No. #4201 and 13522). RKS, NV and DKP acknowledge the financial support given by the ESSO-National Centre for Polar and Ocean Research, Ministry of Earth Sciences, India, to carry this research (RP-077). NV acknowledges CSIR, New Delhi, for providing CSIR-JRF and CSIR-SRF (09/1059(0013)/2017-EMR-I). MD acknowledges DST, New Delhi, for providing INSPIRE Fellowship (IF150105). AKG thanks DST, New Delhi, for the J.C. Bose Fellowship (SR/S2/JCB-80/2011). Funding was provided by the Australian IODP Office and the Australian Research Council (ARC) Basins Genesis Hub (IH130200012) to SJG. The authors declare no conflicts of interest. We are grateful to Editor Ursula Röhl, Associate Editor and two anonymous reviewers for their constructive suggestions that significantly improved the manuscript.

References

Akimoto, K., & Hasegawa, S. (1989). Bathymetric distribution of the Recent benthic foraminifers around Japan—As a contribution to the new paleobathymetric scale. *The Memoirs of the Geological Society of Japan*, 54, 229–240.

- Anderson, C. H., Murray, R. W., Dunlea, A. G., Giosan, L., Kinsley, C. W., McGee, D., & Tada, R. (2018). Climatically Driven Changes in the Supply of Terrigenous Sediment to the East China Sea. *Geochemistry, Geophysics, Geosystems*, 19(8), 2463–2477. <https://doi.org/10.1029/2017GC007339>
- Araújo, H. A. B. de, Dominguez, J. M. L., Machado, A. de J., & Rangel, A. G. de A. N. (2018). Benthic foraminifera distribution in a deltaic clinoform (São Francisco Delta, eastern Brazil): A reference study. *Journal of Marine Systems*, 186, 1–16. <https://doi.org/10.1016/j.jmarsys.2018.05.004>
- Balestra, B., Grunert, P., Ausin, B., Hodell, D., Flores, J.-A., Alvarez-Zarikian, C. A., et al. (2017). Coccolithophore and benthic foraminifera distribution patterns in the Gulf of Cadiz and Western Iberian Margin during Integrated Ocean Drilling Program (IODP) Expedition 339. *Journal of Marine Systems*, 170, 50–67. <https://doi.org/10.1016/j.jmarsys.2017.01.005>
- Ballesteros-Prada, A. (2019). Modern Benthic Foraminifera “Phylum Foraminifera (D’Orbigny 1826)” of the Panama Bight: A Census Report Based on Thanatocoenoses from the Continental Slope. In G. Cusminsky, E. Bernasconi, G. Concheyro (Eds.) *Advances in South American Micropaleontology. Springer Earth System Sciences. Springer, Cham.* (pp. 175–213). https://doi.org/10.1007/978-3-030-02119-1_9
- Barik, S. S., Singh, R. K., Jena, P. S., Tripathy, S., Sharma, K., & Prusty, P. (2019). Spatio-temporal variations in ecosystem and CO₂ sequestration in coastal lagoon: A foraminiferal perspective. *Marine Micropaleontology*, 147, 43–56. <https://doi.org/10.1016/j.marmicro.2019.02.003>
- Bernhard, J. M., Sen Gupta, B. K., & Borne, P. F. (1997). Benthic foraminiferal proxy to estimate dysoxic bottom-water oxygen concentrations; Santa Barbara Basin, U.S. Pacific continental margin. *The Journal of Foraminiferal Research*, 27(4), 301–310. <https://doi.org/10.2113/gsjfr.27.4.301>
- Bhaumik, A. K., Gupta, A. K., Sundar Raj, M., Mohan, K., De, S., & Sarkar, S. (2007). Paleoceanographic evolution of the northeastern Indian ocean during the Miocene: Evidence from deep-sea benthic foraminifera (DSDP Hole 216A). *Indian Journal of Marine Sciences*,

36(4), 332–341.

Black, H. D., Anderson, W. T., & Alvarez Zarikian, C. A. (2018). Data report: organic matter, carbonate, and stable isotope stratigraphy from IODP Expedition 346 Sites U1426, U1427, and U1429. In R. Tada, et al., *Proceedings of the Integrated Ocean Drilling Program*, (Vol. 346). <https://doi.org/10.2204/iodp.proc.346.204.2018>

Bubenshchikova, N. V., Nürnberg, D., Gorbarenko, S. A., & Lembke-Jene, L. (2010). Variations of the oxygen minimum zone of the Okhotsk Sea during the last 50 ka as indicated by benthic foraminiferal and biogeochemical data. *Oceanology*, 50(1), 93–106. <https://doi.org/10.1134/S000143701001011X>

Burkett, A. M., Rathburn, A. E., Elena Pérez, M., Levin, L. A., & Martin, J. B. (2016). Colonization of over a thousand *Cibicidoides wuellerstorfi* (foraminifera: Schwager, 1866) on artificial substrates in seep and adjacent off-seep locations in dysoxic, deep-sea environments. *Deep Sea Research Part I: Oceanographic Research Papers*, 117, 39–50. <https://doi.org/10.1016/j.dsr.2016.08.011>

Charrieau, L. M., Filipsson, H. L., Ljung, K., Chierici, M., Knudsen, K. L., & Kritzberg, E. (2018). The effects of multiple stressors on the distribution of coastal benthic foraminifera: A case study from the Skagerrak-Baltic Sea region. *Marine Micropaleontology*, 139, 42–56. <https://doi.org/10.1016/j.marmicro.2017.11.004>

Chen, C. T. A. (1996). The Kuroshio intermediate water is the major source of nutrients on the East China Sea continental shelf. *Oceanol Acta*, 19.

Chen, C. T. A., Ruo, R., Paid, S. C., Liu, C. T., & Wong, G. T. F. (1995). Exchange of water masses between the East China Sea and the Kuroshio off northeastern Taiwan. *Continental Shelf Research*, 15(1), 19–39. [https://doi.org/10.1016/0278-4343\(93\)E0001-O](https://doi.org/10.1016/0278-4343(93)E0001-O)

Chen, C. T. A., & Wang, S.-L. (1999). Carbon, alkalinity and nutrient budgets on the East China Sea continental shelf. *Journal of Geophysical Research: Oceans*, 104(C9), 20675–20686. <https://doi.org/10.1029/1999JC900055>

Cheng, H., Edwards, R. L., Sinha, A., Spötl, C., Yi, L., Chen, S., et al. (2016). The Asian monsoon

over the past 640,000 years and ice age terminations. *Nature*, 534(7609), 640–646.
<https://doi.org/10.1038/nature18591>

Clemens, S. C., Holbourn, A., Kubota, Y., Lee, K. E., Liu, Z., Chen, G., et al. (2018). Precession-band variance missing from East Asian monsoon runoff. *Nature Communications*, 9(1), 3364.
<https://doi.org/10.1038/s41467-018-05814-0>

Clemens, S. C., Yamamoto, M., Thirumalai, K., Giosan, L., Richey, J. N., Nilsson-Kerr, K., et al. (2021). Remote and local drivers of Pleistocene South Asian summer monsoon precipitation: A test for future predictions. *Science Advances*, 7(23), eabg3848.
<https://doi.org/10.1126/sciadv.abg3848>

Cronin, T. M., Seidenstein, J., Keller, K., McDougall, K., Ruefer, A., & Gemery, L. (2019). The benthic foraminifera *Cassidulina* from the Arctic Ocean: application to paleoceanography and biostratigraphy. *Micropaleontology*, 65(2), 105–125.

Culver, S. J., & Buzas, M. A. (1980). Distribution of recent benthic foraminifera off the North American Atlantic coast. In *Smithsonian Contributions to the Marine Sciences*, (6), 1-512.
<https://doi.org/10.5479/si.01960768.6.1>

Culver, S. J., & Buzas, M. A. (1987). Distribution of Recent benthic foraminifera off the Pacific coast of Mexico and Central America. In *Smithsonian Contributions to the Marine Sciences*, (30), 1–84. <https://doi.org/10.5479/si.01960768.30.1>

Das, Manisha, Singh, R. K., Holbourn, A., Farooq, S. H., Vats, N., & Pandey, D. K. (2021). Paleoceanographic evolution of the Japan Sea during the Pleistocene – A benthic foraminiferal perspective. *Palaeogeography, Palaeoclimatology, Palaeoecology*, 566, 110238. <https://doi.org/10.1016/j.palaeo.2021.110238>

Das, Manisha, Singh, R. K., Vats, N., Holbourn, A., Mishra, S., Farooq, S. H., & Pandey, D. K. (2018). Changes in the distribution of Uvigerinidae species over the past 775 kyr: Implications for the paleoceanographic evolution of the Japan Sea. *Palaeogeography, Palaeoclimatology, Palaeoecology*, 507, 201–213.
<https://doi.org/10.1016/j.palaeo.2018.07.019>

- Das, Manisha, Vats, N., Singh, R. K., Mishra, S., Barik, S. S., Divya, R. V., et al. (2020). Assessing Mid-pleistocene to Holocene Sea-Ice Extent and Carbonate Compensation Depth Fluctuations in the Japan Sea: A Multiproxy Approach. In D. Pandey, M. Ravichandran, N. Nair, (Eds.) *Dynamics of the Earth System: Evolution, Processes and Interactions. Society of Earth Scientists Series. Springer, Cham* (pp. 55–72). https://doi.org/10.1007/978-3-030-40659-2_3
- Das, Moumita, Singh, R. K., Gupta, A. K., & Bhaumik, A. K. (2017). Holocene strengthening of the Oxygen Minimum Zone in the northwestern Arabian Sea linked to changes in intermediate water circulation or Indian monsoon intensity? *Palaeogeography, Palaeoclimatology, Palaeoecology*, 483, 125–135. <https://doi.org/10.1016/j.palaeo.2016.10.035>
- De, S., & Gupta, A. K. (2010). Deep-sea faunal provinces and their inferred environments in the Indian Ocean based on distribution of Recent benthic foraminifera. *Palaeogeography, Palaeoclimatology, Palaeoecology*, 291(3–4), 429–442. <https://doi.org/10.1016/j.palaeo.2010.03.012>
- Diz, P., & Francés, G. (2008). Distribution of live benthic foraminifera in the Ría de Vigo (NW Spain). *Marine Micropaleontology*, 66(3–4), 165–191. <https://doi.org/10.1016/j.marmicro.2007.09.001>
- Duros, P., Fontanier, C., Metzger, E., Pusceddu, A., Cesbron, F., de Stigter, H. C., et al. (2011). Live (stained) benthic foraminifera in the Whittard Canyon, Celtic margin (NE Atlantic). *Deep Sea Research Part I: Oceanographic Research Papers*, 58(2), 128–146. <https://doi.org/10.1016/j.dsr.2010.11.008>
- Fontanier, C., Jorissen, F. ., Licari, L., Alexandre, A., Anschutz, P., & Carbonel, P. (2002). Live benthic foraminiferal faunas from the Bay of Biscay: faunal density, composition, and microhabitats. *Deep Sea Research Part I: Oceanographic Research Papers*, 49(4), 751–785. [https://doi.org/10.1016/S0967-0637\(01\)00078-4](https://doi.org/10.1016/S0967-0637(01)00078-4)
- Fontanier, C., Jorissen, F. J., Chaillou, G., Anschutz, P., Grémare, A., & Griveaud, C. (2005). Live foraminiferal faunas from a 2800m deep lower canyon station from the Bay of Biscay: Faunal

response to focusing of refractory organic matter. *Deep Sea Research Part I: Oceanographic Research Papers*, 52(7), 1189–1227. <https://doi.org/10.1016/j.dsr.2005.01.006>

Fontanier, C., Jorissen, F. J., Lansard, B., Mouret, A., Buscail, R., Schmidt, S., et al. (2008). Live foraminifera from the open slope between Grand Rhône and Petit Rhône Canyons (Gulf of Lions, NW Mediterranean). *Deep Sea Research Part I: Oceanographic Research Papers*, 55(11), 1532–1553. <https://doi.org/10.1016/j.dsr.2008.07.003>

Gallagher, S. J., Kitamura, A., Iryu, Y., Itaki, T., Koizumi, I., & Hoiles, P. W. (2015). The Pliocene to recent history of the Kuroshio and Tsushima Currents: a multi-proxy approach. *Progress in Earth and Planetary Science*, 2(1), 17. <https://doi.org/10.1186/s40645-015-0045-6>

Gallagher, S. J., Sagawa, T., Henderson, A. C. G., Saavedra-Pellitero, M., De Vleeschouwer, D., Black, H., et al. (2018). East Asian Monsoon History and Paleoceanography of the Japan Sea Over the Last 460,000 Years. *Paleoceanography and Paleoclimatology*, 33(7), 683–702. <https://doi.org/10.1029/2018PA003331>

Gallagher, S. J., Wallace, M. W., Li, C. L., Kinna, B., Bye, J. T., Akimoto, K., & Torii, M. (2009). Neogene history of the West Pacific Warm Pool, Kuroshio and Leeuwin currents. *Paleoceanography*, 24(1), PA1206. <https://doi.org/10.1029/2008PA001660>

García-Sanz, I., Usera, J., Guillem, J., Giner-Baixaui, A., & Alberola, C. (2018). Geographical and bathymetric distribution of foraminiferal assemblages from the Alboran Sea (western Mediterranean). *Quaternary International*, 481, 146–156. <https://doi.org/10.1016/j.quaint.2017.11.016>

Garcia, H. E., Boyer, T. P., Locarnini, R. A., Antonov, J. I., Mishonov, A. V., Baranova, O. K., et al. (2013). *World Ocean Atlas 2013. Volume 3: dissolved oxygen, apparent oxygen utilization, and oxygen saturation*. NOAA Atlas NESDIS 75, 3, 27.

Gonzales, M. V., De Almeida, F. K., Costa, K. B., Santarosa, A. C. A., Camillo, E., De Quadros, J. P., & Toledo, F. A. L. (2017). Help index: Hoeglundina elegans preservation index for marine sediments in the western South Atlantic. *The Journal of Foraminiferal Research*, 47(1), 56–69. <https://doi.org/10.2113/gsjfr.47.1.56>

- Gooday, A. J. (1988). A response by benthic Foraminifera to the deposition of phytodetritus in the deep sea. *Nature*, 332(6159), 70–73. <https://doi.org/10.1038/332070a0>
- Gorbarenko, S. A., Southon, J. R., Keigwin, L. D., Cherepanova, M. V., & Gvozdeva, I. G. (2004). Late Pleistocene–Holocene oceanographic variability in the Okhotsk Sea: geochemical, lithological and paleontological evidence. *Palaeogeography, Palaeoclimatology, Palaeoecology*, 209(1–4), 281–301. <https://doi.org/10.1016/j.palaeo.2004.02.013>
- Gorbarenko, S. A., Psheneva, O. Y., Artemova, A. V., Matul', A. G., Tiedemann, R., & Nürnberg, D. (2010). Paleoenvironment changes in the NW Okhotsk Sea for the last 18kyr determined with micropaleontological, geochemical, and lithological data. *Deep Sea Research Part I: Oceanographic Research Papers*, 57(6), 797–811. <https://doi.org/10.1016/j.dsr.2010.04.004>
- Grunert, P., Rosenthal, Y., Jorissen, F., Holbourn, A., Zhou, X., & Piller, W. E. (2018). Mg/Ca-temperature calibration for costate Bulimina species (*B. costata*, *B. inflata*, *B. mexicana*): A paleothermometer for hypoxic environments. *Geochimica et Cosmochimica Acta*, 220, 36–54. <https://doi.org/10.1016/j.gca.2017.09.021>
- Gupta, A. K., Sarkar, S., & Mukherjee, B. (2006). Paleoceanographic changes during the past 1.9 Myr at DSDP Site 238, Central Indian Ocean Basin: Benthic foraminiferal proxies. *Marine Micropaleontology*, 60(2), 157–166. <https://doi.org/10.1016/j.marmicro.2006.04.001>
- Gupta, A. K., Sundar Raj, M., Mohan, K., & De, S. (2008). A major change in monsoon-driven productivity in the tropical Indian Ocean during ca 1.2–0.9 Myr: Foraminiferal faunal and stable isotope data. *Palaeogeography, Palaeoclimatology, Palaeoecology*, 261(3–4), 234–245. <https://doi.org/10.1016/j.palaeo.2008.01.012>
- Gupta, A. K., & Thomas, E. (1999). Latest Miocene-Pleistocene Productivity and Deep-Sea Ventilation in the Northwestern Indian Ocean (Deep Sea Drilling Project Site 219). *Paleoceanography*, 14(1), 62–73. <https://doi.org/10.1029/1998PA900006>
- Gupta, A. K., & Thomas, E. (2003). Initiation of Northern Hemisphere glaciation and strengthening of the northeast Indian monsoon: Ocean Drilling Program Site 758, eastern equatorial Indian Ocean. *Geology*, 31(1), 47. <https://doi.org/10.1130/0091->

7613(2003)031<0047:IONHGA>2.0.CO;2

Haller, C., Hallock, P., Hine, A. C., & Smith, C. G. (2018). Benthic foraminifera from the Carnarvon Ramp reveal variability in Leeuwin Current activity (Western Australia) since the Pliocene. *Marine Micropaleontology*, 142, 25–39. <https://doi.org/10.1016/j.marmicro.2018.05.005>

Hammer, O., Harper, D., & Ryan, P. D. (2001). PAST: paleontological statistic software package for education and data analyses. *Palaeontologia Electronica*, 4.

Harloff, J., & Mackensen, A. (1997). Recent benthic foraminiferal associations and ecology of the Scotia Sea and Argentine Basin. *Marine Micropaleontology*, 31(1–2), 1–29. [https://doi.org/10.1016/S0377-8398\(96\)00059-X](https://doi.org/10.1016/S0377-8398(96)00059-X)

Hayward, B. W., Grenfell, H., & Reid, C. (1997). Foraminiferal associations in Wanganui Bight and Queen Charlotte Sound, New Zealand. *New Zealand Journal of Marine and Freshwater Research*, 31(3), 337–365. <https://doi.org/10.1080/00288330.1997.9516771>

Holbourn, A., Henderson, A. S., & MacLeod, N. (2013). *Atlas of Benthic Foraminifera*. Oxford, UK: Wiley-Blackwell. <https://doi.org/10.1002/9781118452493>

Hu, J., & Wang, X. H. (2016). Progress on upwelling studies in the China seas. *Reviews of Geophysics*, 54(3), 653–673. <https://doi.org/10.1002/2015RG000505>

Hu, D., Cai, W., Ganachaud, A., Kessler, W. S., & Sprintall, J. (2015). Introduction to special section on Western Pacific Ocean Circulation and Climate. *Journal of Geophysical Research: Oceans*, 120(5), 3175–3176. <https://doi.org/10.1002/2015JC010856>

Huang, H.-H. M., Yasuhara, M., Iwatani, H., Yamaguchi, T., Yamada, K., & Mamo, B. (2019). Deep-sea ostracod faunal dynamics in a marginal sea: biotic response to oxygen variability and mid-Pleistocene global changes. *Paleobiology*, 45(1), 85–97. <https://doi.org/10.1017/pab.2018.37>

Ichikawa, H., & Beardsley, R. C. (2002). Review: the current system in the yellow and East China seas. *Journal of Oceanography*, 58. <https://doi.org/10.1023/A:1015876701363>

- Ijiri, A., Wang, L., Oba, T., Kawahata, H., Huang, C. Y., & Huang, C. Y. (2005).
Paleoenvironmental changes in the northern area of the East China Sea during the past 42,000
years. *Palaeogeography, Palaeoclimatology, Palaeoecology*, 219(3–4), 239–261.
<https://doi.org/10.1016/j.palaeo.2004.12.028>
- Irino, T., Tada, R., Ikehara, K., Sagawa, T., Karasuda, A., Kurokawa, S., et al. (2018). Construction
of perfectly continuous records of physical properties for dark-light sediment sequences
collected from the Japan Sea during Integrated Ocean Drilling Program Expedition 346 and
their potential utilities as paleoceanographic studies. *Progress in Earth and Planetary
Science*, 5(1), 23. <https://doi.org/10.1186/s40645-018-0176-7>
- Jian, Z., Wang, L., Kienast, M., Sarnthein, M., Kuhnt, W., Lin, H., & Wang, P. (1999). Benthic
foraminiferal paleoceanography of the South China Sea over the last 40,000 years. *Marine
Geology*, 156(1–4), 159–186. [https://doi.org/10.1016/S0025-3227\(98\)00177-7](https://doi.org/10.1016/S0025-3227(98)00177-7)
- Jiang, D., & Lang, X. (2010). Last Glacial Maximum East Asian Monsoon: Results of PMIP
Simulations. *Journal of Climate*, 23(18), 5030–5038.
<https://doi.org/10.1175/2010JCLI3526.1>
- Ji-lan, S., Yu-qiu, P., & Xiang-san, L. (1994). Kuroshio Intrusion and Taiwan Warm Current. In
Z. Di, L. Yuan-Bo, & Z. Cheng-Kui (Eds.), *Oceanology of China Seas* (pp. 59–70).
Dordrecht: Springer Netherlands. https://doi.org/10.1007/978-94-011-0862-1_7
- Jones, R. W., & Brady, H. B. (1994). *The challenger foraminifera*. Oxford University Press, USA.
- Jorissen, F. J., Wittling, I., Peypouquet, J. P., Rabouille, C., & Relexans, J. C. (1998). Live benthic
foraminiferal faunas off Cape Blanc, NW-Africa: Community structure and microhabitats.
Deep Sea Research Part I: Oceanographic Research Papers, 45(12), 2157–2188.
[https://doi.org/10.1016/S0967-0637\(98\)00056-9](https://doi.org/10.1016/S0967-0637(98)00056-9)
- Jorissen, F. J., Fontanier, C., & Thomas, E. (2007). Chapter Seven Paleoclimatological Proxies
Based on Deep-Sea Benthic Foraminiferal Assemblage Characteristics. In *Developments in
Marine Geology* (pp. 263–325). [https://doi.org/10.1016/S1572-5480\(07\)01012-3](https://doi.org/10.1016/S1572-5480(07)01012-3)
- Kaiho, K., & Nishimura, A. (1992). Distribution of Holocene Benthic Foraminifera in the Izu-

Bonin Arc. In B. Taylor, et al., *Proceedings of the Ocean Drilling Program, Scientific Results*
(Vol. 126, pp. 311–320). Ocean Drilling Program.
<https://doi.org/10.2973/odp.proc.sr.126.138.1992>

Kaiho, K. (1994). Benthic foraminiferal dissolved-oxygen index and dissolved-oxygen levels in
the modern ocean. *Geology*, 22(8), 719. [https://doi.org/10.1130/0091-7613\(1994\)022<0719:BFDIOA>2.3.CO;2](https://doi.org/10.1130/0091-7613(1994)022<0719:BFDIOA>2.3.CO;2)

Kaiho, K. (1999). Effect of organic carbon flux and dissolved oxygen on the benthic foraminiferal
oxygen index (BFOI). *Marine Micropaleontology*, 37(1), 67–76.
[https://doi.org/10.1016/S0377-8398\(99\)00008-0](https://doi.org/10.1016/S0377-8398(99)00008-0)

Kaminski, M. A. (2012). Calibration of the Benthic Foraminiferal Oxygen Index in the Marmara
Sea. *Geological Quarterly*, 56(4), 757–756. <https://doi.org/10.7306/gq.1061>

Kao, S. J., Wu, C.-R., Hsin, Y.-C., & Dai, M. (2006). Effects of sea level change on the upstream
Kuroshio Current through the Okinawa Trough. *Geophysical Research Letters*, 33(16),
L16604. <https://doi.org/10.1029/2006GL026822>

Kao, S. J., Horng, C. S., Hsu, S. C., Wei, K. Y., Chen, J., & Lin, Y. S. (2005). Enhanced deep-
water circulation and shift of sedimentary organic matter oxidation pathway in the Okinawa
Trough since the Holocene. *Geophysical Research Letters*, 32(15), L15609.
<https://doi.org/10.1029/2005GL023139>

Kastens, K., & Mascle, J. (1990). The Geological Evolution of the Tyrrhenian Sea: An
Introduction to the Scientific Results of ODP Leg 107. In K. A. Kastens, et al., *Proceedings*
of the Ocean Drilling Program, Scientific Results (Vol. 107, pp. 3–26). Ocean Drilling
Program. <https://doi.org/10.2973/odp.proc.sr.107.187.1990>

Kawahata, H., & Ohshima, H. (2004). Vegetation and environmental record in the northern East
China Sea during the late Pleistocene. *Global and Planetary Change*, 41.
<https://doi.org/10.1016/j.gloplacha.2004.01.011>

Kender, S., & Kaminski, M. A. (2017). Modern deep-water agglutinated foraminifera from IODP
Expedition 323, Bering Sea: ecological and taxonomic implications. *Journal of*

Micropalaeontology, 195–218. <https://doi.org/10.1144/jmpaleo2016-026>

Kido, Y., Minami, I., Tada, R., Fujine, K., Irino, T., Ikehara, K., & Chun, J.-H. (2007). Orbital-scale stratigraphy and high-resolution analysis of biogenic components and deep-water oxygenation conditions in the Japan Sea during the last 640 kyr. *Palaeogeography, Palaeoclimatology, Palaeoecology*, 247(1–2), 32–49. <https://doi.org/10.1016/j.palaeo.2006.11.020>

Kubota, Y., Kimoto, K., Tada, R., Oda, H., Yokoyama, Y., & Matsuzaki, H. (2010). Variations of East Asian summer monsoon since the last deglaciation based on Mg/Ca and oxygen isotope of planktic foraminifera in the northern East China Sea. *Paleoceanography*, 25(4), PA4205. <https://doi.org/10.1029/2009PA001891>

Kuhnt, W., Hess, S., & Jian, Z. (1999). Quantitative composition of benthic foraminiferal assemblages as a proxy indicator for organic carbon flux rates in the South China Sea. *Marine Geology*, 156(1–4), 123–157. [https://doi.org/10.1016/S0025-3227\(98\)00176-5](https://doi.org/10.1016/S0025-3227(98)00176-5)

Laprida, C., Chapori, N. G., Violante, R. A., & Compagnucci, R. H. (2007). Mid-Holocene evolution and paleoenvironments of the shoreface–offshore transition, north-eastern Argentina: New evidence based on benthic microfauna. *Marine Geology*, 240(1–4), 43–56. <https://doi.org/10.1016/j.margeo.2007.02.001>

Lee, T. N., Johns, W. E., Liu, C.-T., Zhang, D., Zantopp, R., & Yang, Y. (2001). Mean transport and seasonal cycle of the Kuroshio east of Taiwan with comparison to the Florida Current. *Journal of Geophysical Research: Oceans*, 106(C10), 22143–22158. <https://doi.org/10.1029/2000JC000535>

Li, N., Sharifi, A., Chambers, F. M., Ge, Y., Dubois, N., Gao, G., et al. (2021). Linking Holocene East Asian monsoon variability to solar forcing and ENSO activity: Multi-proxy evidence from a peatland in Northeastern China. *The Holocene*, 31(6), 966–982. <https://doi.org/10.1177/0959683621994662>

Li, D., Zhang, J., Huang, D., Wu, Y., & Liang, J. (2002). Oxygen depletion off the Changjiang (Yangtze River) Estuary. *Science in China Series D: Earth Sciences*, 45(12), 1137.

<https://doi.org/10.1360/02yd9110>

Lim, D., Kim, J., Xu, Z., Jeong, K., & Jung, H. (2017). New evidence for Kuroshio inflow and deep-water circulation in the Okinawa Trough, East China Sea: Sedimentary mercury variations over the last 20 kyr. *Paleoceanography*, 32(6), 571–579. <https://doi.org/10.1002/2017PA003116>

Liu, Z., Gan, J., Hu, J., Wu, H., Cai, Z., & Deng, Y. (2021). Progress on circulation dynamics in the East China Sea and southern Yellow Sea: Origination, pathways, and destinations of shelf currents. *Progress in Oceanography*, 193, 102553. <https://doi.org/10.1016/j.pocean.2021.102553>

Liu, K. K., Gong, G.-C., Lin, S., Yang, C.-Y., Wei, C.-L., Pai, S.-C., & Wu, C.-K. (1992). The Year-Round Upwelling at the Shelf Break Near the Northern Tip of Taiwan as Evidenced by Chemical Hydrography. *Terrestrial, Atmospheric and Oceanic Sciences*, 3(3), 243–276. [https://doi.org/10.3319/TAO.1992.3.3.243\(KEEP\)](https://doi.org/10.3319/TAO.1992.3.3.243(KEEP))

Locarnini, R. A., Mishonov, A. V., Baranova, O. K., Boyer, T. P., Zweng, M. M., Garcia, H. E., et al. (2019). *World Ocean Atlas 2018. Volume 1 : Temperature*. NOAA Atlas NESDIS 81, 1, 52.

Loeblich, A. R., & Tappan, H. (1988). *Foraminiferal Genera and Their Classification*. Boston, MA: Springer US. <https://doi.org/10.1007/978-1-4899-5760-3>

Lutze, G. F. (1979). Benthic Foraminifers at Site 397: Faunal Fluctuations and Ranges in the Quaternary. In *Initial Reports of the Deep Sea Drilling Project, 47 Pt. 1* (pp. 419–431). <https://doi.org/10.2973/dsdp.proc.47-1.111.1979>

Lutze, G. F., & Thiel, H. (1989). Epibenthic foraminifera from elevated microhabitats; *Cibicidoides wuellerstorfi* and *Planulina ariminensis*. *The Journal of Foraminiferal Research*, 19(2), 153–158. <https://doi.org/10.2113/gsjfr.19.2.153>

Ma, R., Sépulcre, S., Licari, L., Bassinot, F., Liu, Z., Tisnérat-Laborde, N., et al. (2019). Changes in Intermediate Circulation in the Bay of Bengal Since the Last Glacial Maximum as Inferred From Benthic Foraminifera Assemblages and Geochemical Proxies. *Geochemistry*,

- 882 *Geophysics, Geosystems*, 20(3), 1592–1608. <https://doi.org/10.1029/2018GC008179>
- 883 Mackensen, A., & Hald, M. (1988). *Cassidulina teretis* Tappan and *C. laevigata* d'Orbigny; their
884 modern and late Quaternary distribution in northern seas. *The Journal of Foraminiferal*
885 *Research*, 18(1), 16–24. <https://doi.org/10.2113/gsjfr.18.1.16>
- 886 Mackensen, A., Schmiedl, G., Harloff, J., & Giese, M. (1995). Deep-sea foraminifera in the South
887 Atlantic ocean: Ecology and assemblage generation. *Micropaleontology*, 41(4), 342–358.
888 <https://doi.org/10.2307/1485808>
- 889 Martínez-García, B., Pascual, A., Rodríguez-Lázaro, J., & Bodego, A. (2013). Recent benthic
890 foraminifers of the Basque continental shelf (Bay of Biscay, northern Spain): Oceanographic
891 implications. *Continental Shelf Research*, 66, 105–122.
892 <https://doi.org/10.1016/j.csr.2013.07.006>
- 893 Martins, V., Dubert, J., Jouanneau, J.-M., Weber, O., da Silva, E. F., Patinha, C., et al. (2007). A
894 multiproxy approach of the Holocene evolution of shelf–slope circulation on the NW Iberian
895 Continental Shelf. *Marine Geology*, 239(1–2), 1–18.
896 <https://doi.org/10.1016/j.margeo.2006.11.001>
- 897 Matsuzaki, K. M., Itaki, T., & Kimoto, K. (2016). Vertical distribution of polycystine radiolarians
898 in the northern East China Sea. *Marine Micropaleontology*, 125, 66–84.
899 <https://doi.org/10.1016/j.marmicro.2016.03.004>
- 900 Matsuzaki, K. M., Itaki, T., & Tada, R. (2019). Paleooceanographic changes in the Northern East
901 China Sea during the last 400 kyr as inferred from radiolarian assemblages (IODP Site
902 U1429). *Progress in Earth and Planetary Science*, 6(1), 22. [https://doi.org/10.1186/s40645-](https://doi.org/10.1186/s40645-019-0256-3)
903 019-0256-3
- 904 Mazumder, A., & Nigam, R. (2014). Bathymetric preference of four major genera of rectilinear
905 benthic foraminifera within oxygen minimum zone in Arabian Sea off central west coast of
906 India. *Journal of Earth System Science*, 123(3), 633–639. [https://doi.org/10.1007/s12040-](https://doi.org/10.1007/s12040-014-0419-y)
907 014-0419-y
- 908 McGann, M., & Conrad, J. E. (2018). Faunal and stable isotopic analyses of benthic foraminifera

from the Southeast Seep on Kimki Ridge offshore southern California, USA. *Deep Sea Research Part II: Topical Studies in Oceanography*, 150, 92–117. <https://doi.org/10.1016/j.dsr2.2018.01.011>

Murray, J. W. (2006). Ecology and Applications of Benthic Foraminifera. In *Ecology and applications of benthic foraminifera*, Cambridge University Press. Cambridge: Cambridge University Press. <https://doi.org/10.1017/CBO9780511535529>

Nardelli, M. P., Barras, C., Metzger, E., Mouret, A., Filipsson, H. L., Jorissen, F., & Geslin, E. (2014). Experimental evidence for foraminiferal calcification under anoxia. *Biogeosciences*, 11(14), 4029–4038. <https://doi.org/10.5194/bg-11-4029-2014>

Pahnke, K. (2003). 340,000-Year Centennial-Scale Marine Record of Southern Hemisphere Climatic Oscillation. *Science*, 301(5635), 948–952. <https://doi.org/10.1126/science.1084451>

Pascual, A., Rodríguez-Lázaro, J., Martínez-García, B., & Varela, Z. (2020). Palaeoceanographic and palaeoclimatic changes during the last 37,000 years detected in the SE Bay of Biscay based on benthic foraminifera. *Quaternary International*, 566–567, 323–336. <https://doi.org/10.1016/j.quaint.2020.03.043>

Patarroyo, G. D., & Martínez, J. I. (2015). Late quaternary sea bottom conditions in the southern Panama basin, Eastern Equatorial Pacific. *Journal of South American Earth Sciences*, 63, 346–359. <https://doi.org/10.1016/j.jsames.2015.07.010>

Pérez-Asensio, J. N., Aguirre, J., & Rodríguez-Tovar, F. J. (2017). The effect of bioturbation by polychaetes (Opheliidae) on benthic foraminiferal assemblages and test preservation. *Palaeontology*, 60(6), 807–827. <https://doi.org/10.1111/pala.12317>

Phleger, F. B., & Soutar, A. (1973). Production of Benthic Foraminifera in Three East Pacific Oxygen Minima. *Micropaleontology*, 19(1), 110. <https://doi.org/10.2307/1484973>

Qi, J., Yin, B., Zhang, Q., Yang, D., & Xu, Z. (2017). Seasonal variation of the Taiwan Warm Current Water and its underlying mechanism. *Chinese Journal of Oceanology and Limnology*, 35(5), 1045–1060. <https://doi.org/10.1007/s00343-017-6018-4>

- 935 Rathburn, A. E., & Corliss, B. H. (1994). The ecology of living (stained) deep-sea benthic
936 foraminifera from the Sulu Sea. *Paleoceanography*, 9(1), 87–150.
937 <https://doi.org/10.1029/93PA02327>
- 938 Rathburn, A. E., Willingham, J., Ziebis, W., Burkett, A. M., & Corliss, B. H. (2018). A New
939 biological proxy for deep-sea paleo-oxygen: Pores of epifaunal benthic foraminifera.
940 *Scientific Reports*, 8(1), 9456. <https://doi.org/10.1038/s41598-018-27793-4>
- 941 Reolid, M., Rodríguez-Tovar, F. J., & Nagy, J. (2012). Ecological replacement of Valanginian
942 agglutinated foraminifera during a maximum flooding event in the Boreal realm
943 (Spitsbergen). *Cretaceous Research*, 33(1), 196–204.
944 <https://doi.org/10.1016/j.cretres.2011.10.003>
- 945 Revelle, W. (2019). *psych: Procedures for Psychological, Psychometric, and Personality*
946 *Research*. Northwestern University, Evanston, Illinois. R package version 1.9.12,
947 <https://cran.r-project.org/package=psych>.
- 948 Rostami, M. A., Frontalini, F., Leckie, R. M., Coccioni, R., Font, E., & Balmaki, B. (2020).
949 Benthic Foraminifera Across the Cretaceous/Paleogene Boundary in the Eastern Tethys
950 (Northern Alborz, Galanderud Section): Extinction Pattern and Paleoenvironmental
951 Reconstruction. *Journal of Foraminiferal Research*, 50(1), 25–40.
952 <https://doi.org/10.2113/gsjfr.50.1.25>
- 953 RStudio Team. (2020). *RStudio: Integrated Development Environment for R*. Boston, MA.
954 <http://www.rstudio.com/>
- 955 Ryan, W. B. F., Carbotte, S. M., Coplan, J. O., O'Hara, S., Melkonian, A., Arko, R., et al. (2009).
956 Global Multi-Resolution Topography synthesis. *Geochemistry, Geophysics, Geosystems*,
957 10(3), Q03014. <https://doi.org/10.1029/2008GC002332>
- 958 Saavedra-Pellitero, M., Baumann, K.-H., Gallagher, S. J., Sagawa, T., & Tada, R. (2019).
959 Paleooceanographic evolution of the Japan Sea over the last 460 kyr – A coccolithophore
960 perspective. *Marine Micropaleontology*, 152, 101720.
961 <https://doi.org/10.1016/j.marmicro.2019.01.001>

- 962 Sagawa, T., Nagahashi, Y., Satoguchi, Y., Holbourn, A., Itaki, T., Gallagher, S. J., et al. (2018).
963 Integrated tephrostratigraphy and stable isotope stratigraphy in the Japan Sea and East China
964 Sea using IODP Sites U1426, U1427, and U1429, Expedition 346 Asian Monsoon. *Progress*
965 *in Earth and Planetary Science*, 5(1), 18. <https://doi.org/10.1186/s40645-018-0168-7>
- 966 Saravanan, P., Gupta, A. K., Zheng, H., Panigrahi, M. K., & Prakasam, M. (2019). Late Holocene
967 long arid phase in the Indian subcontinent as seen in shallow sediments of the eastern Arabian
968 Sea. *Journal of Asian Earth Sciences*, 181, 103915.
969 <https://doi.org/10.1016/j.jseaes.2019.103915>
- 970 Sarkar, S., & Gupta, A. K. (2014). Late Quaternary productivity changes in the equatorial Indian
971 Ocean (ODP Hole 716A). *Palaeogeography, Palaeoclimatology, Palaeoecology*, 397, 7–19.
972 <https://doi.org/10.1016/j.palaeo.2013.12.002>
- 973 Schmiedl, G., Mackensen, A., & Müller, P. J. (1997). Recent benthic foraminifera from the eastern
974 South Atlantic Ocean: Dependence on food supply and water masses. *Marine*
975 *Micropaleontology*, 32(3–4), 249–287. [https://doi.org/10.1016/S0377-8398\(97\)00023-6](https://doi.org/10.1016/S0377-8398(97)00023-6)
- 976 Schmiedl, G, de Bovée, F., Buscail, R., Charrière, B., Hemleben, C., Medernach, L., & Picon, P.
977 (2000). Trophic control of benthic foraminiferal abundance and microhabitat in the bathyal
978 Gulf of Lions, western Mediterranean Sea. *Marine Micropaleontology*, 40(3), 167–188.
979 [https://doi.org/10.1016/S0377-8398\(00\)00038-4](https://doi.org/10.1016/S0377-8398(00)00038-4)
- 980 Schmiedl, G., & Leuschner, D. C. (2005). Oxygenation changes in the deep western Arabian Sea
981 during the last 190,000 years: Productivity versus deep-water circulation. *Paleoceanography*,
982 20(2), PA2008. <https://doi.org/10.1029/2004PA001044>
- 983 Schmiedl, G., & Mackensen, A. (1997). Late Quaternary paleoproductivity and deep water
984 circulation in the eastern South Atlantic Ocean: Evidence from benthic foraminifera.
985 *Palaeogeography, Palaeoclimatology, Palaeoecology*, 130(1–4), 43–80.
986 [https://doi.org/10.1016/S0031-0182\(96\)00137-X](https://doi.org/10.1016/S0031-0182(96)00137-X)
- 987 Schulz, M., & Mudelsee, M. (2002). REDFIT: estimating red-noise spectra directly from unevenly
988 spaced paleoclimatic time series. *Computers & Geosciences*, 28(3), 421–426.

[https://doi.org/10.1016/S0098-3004\(01\)00044-9](https://doi.org/10.1016/S0098-3004(01)00044-9)

Schweizer, M. (2006). *Evolution and molecular phylogeny of Cibicides and Uvigerina (Rotalida, Foraminifera)*. Utrecht University.

Scott, D. B., Schell, T., Rochon, A., & Blasco, S. (2008). Modern benthic foraminifera in the surface sediments of the Beaufort shelf, slope and Mackenzie trough, Beaufort sea, Canada: taxonomy and summary of surficial distributions. *The Journal of Foraminiferal Research*, 38(3), 228–250. <https://doi.org/10.2113/gsjfr.38.3.228>

Scott, D. B., Takayanagi, Y., Hasegawa, S., & Saito, T. (2000). Illustration and taxonomic reevaluation of neogene foraminifera described from Japan. *Palaeontologia Electronica*, 3(2), 1–41.

Sen Gupta, B. K., & Machain-Castillo, M. L. (1993). Benthic foraminifera in oxygen-poor habitats. *Marine Micropaleontology*, 20(3–4), 183–201. [https://doi.org/10.1016/0377-8398\(93\)90032-S](https://doi.org/10.1016/0377-8398(93)90032-S)

Shannon, C. E., & Weaver, W. (1949). *The mathematical theory of communication*. Urbana: University of Illinois Press.

Singh, A. D., Rai, A. K., Tiwari, M., Naidu, P. D., Verma, K., Chaturvedi, M., et al. (2015). Fluctuations of Mediterranean Outflow Water circulation in the Gulf of Cadiz during MIS 5 to 7: Evidence from benthic foraminiferal assemblage and stable isotope records. *Global and Planetary Change*, 133, 125–140. <https://doi.org/10.1016/j.gloplacha.2015.08.005>

Singh, R. K., Gupta, A. K., Das, M., & Flower, B. P. (2021). Paleooceanographic shift during the Plio-Pleistocene in the southeastern Indian Ocean: Linkages with Northern Hemisphere glaciation and Indian monsoon variability. *Palaeogeography, Palaeoclimatology, Palaeoecology*, 571, 110374. <https://doi.org/10.1016/j.palaeo.2021.110374>

Singh, R. K., & Gupta, A. K. (2004). Late Oligocene–Miocene paleooceanographic evolution of the southeastern Indian Ocean: evidence from deep-sea benthic foraminifera (ODP Site 757). *Marine Micropaleontology*, 51(1–2), 153–170. <https://doi.org/10.1016/j.marmicro.2003.10.003>

- 1016 Singh, R. K., & Gupta, A. K. (2010). Deep-sea benthic foraminiferal changes in the eastern Indian
1017 Ocean (ODP Hole 757B): Their links to deep Indonesian (Pacific) flow and high latitude
1018 glaciation during the Neogene. *Episodes, International Union of Geological Sciences*, 33(2),
1019 74–82. <https://doi.org/10.18814/epiiugs/2010/v33i2/001>
- 1020 Smith, P. B. (1964). Ecology of benthonic species. *Geological Survey Professional Paper*, 429-B,
1021 B1–B55.
- 1022 Spratt, R. M., & Lisiecki, L. E. (2016). A Late Pleistocene sea level stack. *Climate of the Past*,
1023 12(4), 1079–1092. <https://doi.org/10.5194/cp-12-1079-2016>
- 1024 Sun, Y., Wu, H., Kageyama, M., Ramstein, G., Li, L. Z. X., Tan, N., et al. (2021). The contrasting
1025 effects of thermodynamic and dynamic processes on East Asian summer monsoon
1026 precipitation during the Last Glacial Maximum: a data-model comparison. *Climate*
1027 *Dynamics*, 56(3–4), 1303–1316. <https://doi.org/10.1007/s00382-020-05533-7>
- 1028 Tada, R., Murray, R. W., Alvarez Zarikian, C. A., Anderson, W. T. J., Bassetti, M.-A., Brace, B.
1029 J., et al. (2015). Sites U1428 and U1429. In *Proceedings of the Integrated Ocean Drilling*
1030 *Program*, (Vol. 346). <https://doi.org/10.2204/iodp.proc.346.109.2015>
- 1031 Tada, R., Irino, T., & Koizumi, I. (1999). Land-ocean linkages over orbital and millennial
1032 timescales recorded in Late Quaternary sediments of the Japan Sea. *Paleoceanography*,
1033 14(2), 236–247. <https://doi.org/10.1029/1998PA900016>
- 1034 Takata, H., Kim, H. J., Asahi, H., Thomas, E., Yoo, C. M., Chi, S. B., & Khim, B.-K. (2019).
1035 Central Equatorial Pacific benthic foraminifera during the mid-Brunhes dissolution interval:
1036 Ballasting of particulate organic matter by biogenic silica and carbonate. *Quaternary Science*
1037 *Reviews*, 210, 64–79. <https://doi.org/10.1016/j.quascirev.2019.02.030>
- 1038 Takata, H., Nishida, N., Ikehara, K., Katsuki, K., & Khim, B.-K. (2018). Mid-Holocene forcing of
1039 the Tsushima Warm Current to the coastal environments in southwestern Japan with a view
1040 to foraminiferal faunas. *Quaternary International*, 482, 56–66.
1041 <https://doi.org/10.1016/j.quaint.2018.04.024>
- 1042 Taylor, M. A., Hendy, I. L., & Chappaz, A. (2017). Assessing oxygen depletion in the Northeastern

- 1043 Pacific Ocean during the last deglaciation using I/Ca ratios from multiple benthic
1044 foraminiferal species. *Paleoceanography*, 32(8), 746–762.
1045 <https://doi.org/10.1002/2016PA003062>
- 1046 Van Morkhoven, F. P. C. M., Berggren, W. A., Edwards, A. S., & Oertli, H. J. (1986). *Cenozoic*
1047 *cosmopolitan deep-water benthic Foraminifera*. Pau: Elf Aquitaine.
- 1048 Vats, N., Mishra, S., Singh, R. K., Gupta, A. K., & Pandey, D. K. (2020). Paleooceanographic
1049 changes in the East China Sea during the last ~400 kyr reconstructed using planktic
1050 foraminifera. *Global and Planetary Change*, 103173.
1051 <https://doi.org/10.1016/j.gloplacha.2020.103173>
- 1052 Vats, N., Singh, R. K., Das, M., Holbourn, A., Gupta, A. K., Gallagher, S. J., & Pandey, D. K.
1053 (2021). Linkages between East China Sea Deep-sea Oxygenation and the Variability of the
1054 East Asian Summer Monsoon and Kuroshio Current over last 400,000 years [Data Set].
1055 *Mendeley Data*, V1. <http://dx.doi.org/10.17632/gcsgc2byps.1>
- 1056 Verma, S., Gupta, A. K., & Singh, R. K. (2013). Variations in deep-sea benthic foraminifera at
1057 ODP Hole 756B, southeastern Indian Ocean: Evidence for changes in deep ocean circulation.
1058 *Palaeogeography, Palaeoclimatology, Palaeoecology*, 376, 172–183.
1059 <https://doi.org/10.1016/j.palaeo.2013.02.034>
- 1060 Wang, B. (2009). Hydromorphological mechanisms leading to hypoxia off the Changjiang estuary.
1061 *Marine Environmental Research*, 67(1), 53–58.
1062 <https://doi.org/10.1016/j.marenvres.2008.11.001>
- 1063 Wang, B., Wei, Q., Chen, J., & Xie, L. (2012). Annual cycle of hypoxia off the Changjiang
1064 (Yangtze River) Estuary. *Marine Environmental Research*, 77, 1–5.
1065 <https://doi.org/10.1016/j.marenvres.2011.12.007>
- 1066 Wang, J., Chang, F., Li, T., Sun, H., Cui, Y., & Liu, T. (2020). The evolution of the Kuroshio
1067 Current over the last 5 million years since the Pliocene: Evidence from planktonic
1068 foraminiferal faunas. *Science China Earth Sciences*, 63(11), 1714–1729.
1069 <https://doi.org/10.1007/s11430-019-9641-9>

- 1070 Wang, N., Huang, B.-Q., Dong, Y.-T., & Xie, X. (2018). The evolution of deep-water dissolved
1071 oxygen in the northern South China Sea since 400 ka. *Palaeoworld*, 27(2), 301–308.
1072 <https://doi.org/10.1016/j.palwor.2017.11.001>
- 1073 Wei, H., He, Y., Li, Q., Liu, Z., & Wang, H. (2007). Summer hypoxia adjacent to the Changjiang
1074 Estuary. *Journal of Marine Systems*, 67(3–4), 292–303.
1075 <https://doi.org/10.1016/j.jmarsys.2006.04.014>
- 1076 Watanabe, S., Tada, R., Ikehara, K., Fujine, K., & Kido, Y. (2007). Sediment fabrics, oxygenation
1077 history, and circulation modes of Japan Sea during the Late Quaternary. *Palaeogeography*,
1078 *Palaeoclimatology*, *Palaeoecology*, 247(1–2), 50–64.
1079 <https://doi.org/10.1016/j.palaeo.2006.11.021>
- 1080 Wu, C.-R., Lu, H.-F., & Chao, S.-Y. (2008). A numerical study on the formation of upwelling off
1081 northeast Taiwan. *Journal of Geophysical Research*, 113(C8), C08025.
1082 <https://doi.org/10.1029/2007JC004697>
- 1083 Xie, C., Jian, Z., & Zhao, Q. (1995). *Paleogeographic maps of the China seas at the last glacial*
1084 *maximum*. Shanghai: UNESCO/IOC Publications.
- 1085 Zhang, J., Liu, S. M., Ren, J. L., Wu, Y., & Zhang, G. L. (2007). Nutrient gradients from the
1086 eutrophic Changjiang (Yangtze River) Estuary to the oligotrophic Kuroshio waters and re-
1087 evaluation of budgets for the East China Sea Shelf. *Progress in Oceanography*, 74(4), 449–
1088 478. <https://doi.org/10.1016/j.pocean.2007.04.019>
- 1089 Zhao, B., Yan, X., Wang, Z., Shi, Y., Chen, Z., Xie, J., et al. (2018). Sedimentary evolution of the
1090 Yangtze River mouth (East China Sea) over the past 19,000 years, with emphasis on the
1091 Holocene variations in coastal currents. *Palaeogeography*, *Palaeoclimatology*,
1092 *Palaeoecology*, 490, 431–449. <https://doi.org/10.1016/j.palaeo.2017.11.023>
- 1093 Zhao, D., Wan, S., Song, Z., Gong, X., Zhai, L., Shi, X., & Li, A. (2019). Asynchronous Variation
1094 in the Quaternary East Asian Winter Monsoon Associated With the Tropical Pacific ENSO-
1095 Like System. *Geophysical Research Letters*, 46(12), 6955–6963.
1096 <https://doi.org/10.1029/2019GL083033>

- 1097 Zhao, D., Wan, S., Toucanne, S., Clift, P. D., Tada, R., Révillon, S., et al. (2017). Distinct control
1098 mechanism of fine-grained sediments from Yellow River and Kyushu supply in the northern
1099 Okinawa Trough since the last glacial. *Geochemistry, Geophysics, Geosystems*, 18(8), 2949–
1100 2969. <https://doi.org/10.1002/2016GC006764>
- 1101 Zheng, X., Li, A., Kao, S., Gong, X., Frank, M., Kuhn, G., et al. (2016). Synchronicity of Kuroshio
1102 Current and climate system variability since the Last Glacial Maximum. *Earth and Planetary
1103 Science Letters*, 452, 247–257. <https://doi.org/10.1016/j.epsl.2016.07.028>
- 1104 Zhou, P., Song, X., Yuan, Y., Cao, X., Wang, W., Chi, L., & Yu, Z. (2018a). Water Mass Analysis
1105 of the East China Sea and Interannual Variation of Kuroshio Subsurface Water Intrusion
1106 Through an Optimum Multiparameter Method. *Journal of Geophysical Research: Oceans*,
1107 123(5), 3723–3738. <https://doi.org/10.1029/2018JC013882>
- 1108 Zhou, P., Song, X., Yuan, Y., Wang, W., Chi, L., Cao, X., & Yu, Z. (2018b). Intrusion of the
1109 Kuroshio Subsurface Water in the southern East China Sea and its variation in 2014 and 2015
1110 traced by dissolved inorganic iodine species. *Progress in Oceanography*, 165, 287–298.
1111 <https://doi.org/10.1016/j.pocean.2018.06.011>
- 1112 Zhou, Y., Chen, F., Wu, C., Yu, S., & Zhuang, C. (2016). Palaeoproductivity linked to monsoon
1113 variability in the northern slope of the South China Sea from the last 290 kyr: evidence of
1114 benthic foraminifera from Core SH7B. *Geological Society, London, Special Publications*,
1115 429(1), 197–210. <https://doi.org/10.1144/SP429.10>
- 1116 Zhu, Z.-Y., Zhang, J., Wu, Y., Zhang, Y.-Y., Lin, J., & Liu, S.-M. (2011). Hypoxia off the
1117 Changjiang (Yangtze River) Estuary: Oxygen depletion and organic matter decomposition.
1118 *Marine Chemistry*, 125(1–4), 108–116. <https://doi.org/10.1016/j.marchem.2011.03.005>
- 1119 Zwaan, G. J. van der, Jorissen, F. J., Verhallen, P. J. J. M., & Daniels, C. H. von. (1986). Atlantic-
1120 European oligocene to recent uvigerina : taxonomy, paleoecology and paleobiogeography.
1121 *Utrecht Micropaleontological Bulletins*, 35.
- 1122 Zweng, M. M., Reagan, J. R., Seidov, D., Boyer, T. P., Antonov, J. I., Locarnini, R. A., et al.
1123 (2019). *World Ocean Atlas 2018, Volume 2: Salinity*. NOAA Atlas NESDIS 82, 2, 50.